Materials Today Bio 28 (2024) 101220

Contents lists available at ScienceDirect

Materials Today Bio

journal homepage: www.journals.elsevier.com/materials-today-bio

Recombinant humanized type III collagen inhibits ovarian cancer and induces protective anti-tumor immunity by regulating autophagy through GSTP1

Hui Zeng [a,1], Hu Li [a,1], Li Wang [a], Shuang You [a], Shuaibin Liu [a], Xiaojing Dong [a], Fan He [a,b,c], Jingcong Dai [a], Quan Wei [a], Zhiyong Dong [a], Yanli Zhang [f], Jingbo Yang [e], Xia Yang [d], Jian Wang [d], Lina Hu [a,b,c,*]

[a] Department of Obstetrics and Gynecology, The Second Affiliated Hospital, Chongqing Medical University, Chongqing 400010, China
[b] Joint International Research Lab for Reproduction and Development, Ministry of Education, Chongqing 400010, China
[c] Reproduction and Stem Cell Therapy Research Center of Chongqing, Chongqing 400010, China
[d] Shanxi Key Laboratory of Functional Proteins, Shanxi Jinbo Bio-Pharmaceutical Co., Ltd., Taiyuan 030032, Shanxi, China
[e] University College London, 19 Gordon Square, Bloomsbury, London, WC1H 0AW, England, UK
[f] Imaging Core Facility, Technology Center for Protein Science, Tsinghua University, Beijing 100084, China

ARTICLE INFO

Keywords:
Recombinant humanized type III collagen
Ovarian cancer cells
Autophagy
GSTP1
Anti-tumor immunity

ABSTRACT

Ovarian cancer (OC) is one of the leading causes of death from malignancy in women and lacks safe and efficient treatment. The novel biomaterial, recombinant humanized collagen type III (rhCOLIII), has been reported to have various biological functions, but its role in OC is unclear. This study aimed to reveal the function and mechanism of action of rhCOLIII in OC. We developed an injectable recombinant human collagen (rhCOL)-derived material with a molecular weight of 45 kDa, with a stable triple helix structure, high biocompatibility, water solubility and biosafety. The anti-tumor activity of rhCOLIII was comprehensively evaluated through *in vitro and in vivo* experiments. *In vitro*, our results showed that rhCOLIII inhibited the proliferation, migration, and invasion of ovarian cancer cells (OCCs), and induced apoptosis. In addition, rhCOLIII not only inhibited autophagy of OCCs but also increased the expression of MHC-1 molecule within OCCs. To further elucidate the mechanism of rhCOLIII in OC, we conducted joint analysis of RNA-Seq and proteomics, and found that rhCOLIII exerted anti-tumor function and autophagy inhibition by downregulating Glutathione S-transferase P1 (GSTP1). Furthermore, various rescue experiments were designed to demonstrate that rhCOLIII suppressed autophagy and proliferation of OCCs by mediating GSTP1. *In vivo*, we found that rhCOLIII could inhibit tumor growth and promote $CD8^+$ T cell infiltration. Our results indicate that rhCOLIII has great anti-tumor potential activity in OC, and induces protective anti-tumor immunity by regulating autophagy through GSTP1. These findings illustrate the potential therapeutic prospects of rhCOLIII for OC treatment.

1. Introduction

Currently, ovarian cancer (OC) is the first deadly tumor of the female reproductive system because of the difficulty of early diagnosis, high rates of recurrence and metastasis, and a low 5-year overall survival rate [1]. The standard treatment for OC, involves tumor cytoreductive surgery combined with chemotherapy, but the therapeutic effect is greatly impaired by chemoresistance [2]. Accordingly, there is an urgent need to improve therapeutic approaches to OC.

In recent years, there has been a notable advance in the development of new biomaterials for diagnostic and therapeutic strategies against cancer, particularly new nanomaterials and hydrogels [3,4]. However, unresolved problems impede the clinical application of these biomaterials. For example, various anti-tumor nanomaterials, including

* Corresponding author. Department of Obstetrics and Gynecology, The Second Affiliated Hospital, Chongqing Medical University, Chongqing 400010, China.
E-mail addresses: zenghui951224@163.com (H. Zeng), lihu1007@qq.com (H. Li), 916398056@qq.com (L. Wang), 399764227@qq.com (S. You), dr.hefan@cqmu.edu.cn (F. He), cqmudjc@126.com (J. Dai), 15084302534@163.com (Q. Wei), 2029128501@qq.com (Z. Dong), yanlizhang12@mail.tisnghua.edu.cn (Y. Zhang), jingboyangsharon@outlook.com (J. Yang), qiu1009@163.com (X. Yang), wj7520991@163.com (J. Wang), cqhulina@hospital.cqmu.edu.cn (L. Hu).
[1] These authors contributed equally to this work.

https://doi.org/10.1016/j.mtbio.2024.101220
Received 6 June 2024; Received in revised form 19 August 2024; Accepted 31 August 2024
Available online 1 September 2024

lipidic, inorganic, agents and nanocarriers, have shown the limitations of rapid drug release, non-specific targeting, lack of stability and toxicity. Although hybrid nanomaterials have raised hopes of successful therapeutic outcomes, there remain some problems hindering their clinical translation in reproducibility of size, coating, and encapsulation efficiency of hybrid nanomaterials [5,6]. More importantly, most of the above-mentioned biomaterials do not exert anti-tumor effects but are more often used for drug-loading. Therefore, the development of safe, efficient, cost-effective and clinically transferrable anti-cancer biomaterials was priority.

Recently, the tumor microenvironment (TME) has become an important focus of research. Collagen, as one of the most abundant components of the extracellular matrix (ECM), has been increasingly recognized as involved in TME remodeling, tumor metabolism and immunity [7,8]. Recent studies have reported that type III collagen may be used as a physical barrier preventing the proliferation and metastasis of breast cancer tumor cells, and promoting apoptosis and dormancy of tumor cells [9]. In addition, loss of type III collagen in elderly OC patients was approved to result in an increased risk of peritoneal metastases [10]. It follows that, collagen type III may be a promising therapeutic strategy in anti-cancer treatment.

Since the 1880s, collagen has been investigated and increasingly utilized with improvements in bioengineering technology [11]. However, traditional collagen is mostly derived from animals, is difficult to be dissolved in water, with high risks of virus transmission, potential immunogenicity and high production costs, which greatly limits its clinical application [12]. In order to improve the biological and structural properties of traditional collagen, we have developed a novel recombinant humanized collagen type III (rhCOLIII) using gene recombination and biosynthesis technology. The amino acid sequence, repeated 16 times in tandem, is a specific functional domain of human collagen, showing a 164.88° flexible triple helix structure [13]. Furthermore, it has lower antigenicity, better biodegradability, higher biological activity, and more stable structural properties than animal-derived type III collagen or full-length human type III collagen [14]. In addition, our previous researches affirmed that rhCOLIII had favorable material-cell interactions and was able to treat vaginal atrophy, pelvic floor dysfunction, and chronic endometritis [15–17]. More importantly, rhCOLIII showed beneficial activity in anti-breast cancer cells, although the specific mechanism of action was not clear [18]. Therefore, due to the favorable biological material properties of rhCOLIII, it is worthy of more research for clinical application.

Our study aimed to further explore whether rhCOLIII exerted anticancer activity in OC and the potential specific mechanisms involved. To study the effects of rhCOLIII on OC cells, we evaluated the proliferation, migration and invasion of OC cells treated with rhCOLIII *in vitro*. Furthermore, we employed RNA-Seq analysis and proteomics to explore the mechanism of action of rhCOLIII in OC. Subsequently, a mouse model of subcutaneous transplantation of OC was established for an *in vivo* study and to evaluate the ability in immunity regulation. Therefore, we hope to explore more functions of rhCOLIII in OC through *in vitro and in vivo* experiments and provide a new direction for its treatment.

2. Materials and methods

2.1. Preparation of the rhCOLIII

Based on the Gly 483-Pro512 fragment of the human type III collagen α1 chain, Shanxi Jinbo Biopharmaceutical Co., Ltd manufactured, under GMP conditions, a new type of biomaterial rhCOLIII, at a dose of 4 mg per vial. Briefly, rhCOLIII consists of the triple-helix fragment of hCOLIIIα3, Gly483-Pro512, which has undergone 16 tandem repeats to form the final rhCOLIII structure. The rhCOLIII gene was transformed in *Escherichia coli* (BL21(DE3)) through recombinant expression vectors. Finally, after induction by isopropylthio-β-galactoside, we used nickel-chelate and anion-exchange chromatography to purify the expressed protein.

2.2. Cell culture

The human ovarian cancer cell lines A2780 and SKOV3, were purchased from Procell (Wuhan, China), and authenticated by short tandem repeat (STR) analysis. A2780 and SKOV3 were respectively cultured in DMEM and McCoy's 5A medium (Gibco, UK) with 10 % fetal bovine serum (PAN, Germany) and 1 % penicillin-streptomycin solution (Beyotime, C0222) in a 5 % CO_2 incubator at 37 °C. Due to its excellent water solubility, rhCOLIII can be directly dissolved in cell culture media. The control (or NC) group contained no added rhCOLIII. The *in vitro* experiments included subgroups with different concentrations of rhCOLIII (0.5, 1, 2, 4, and 8 mg/ml).

2.3. Cell transfection

A2780 cells were transfected with GSTP1 small interfering RNA (siRNA), ATG3 siRNA, ATG5 siRNA, NBR1 siRNA and P62 siRNA (TSINGKE, China), or negative control, using LipofectamineTM 3000 Transfection Reagent (Invitrogen, USA) according to the manufacturer's instructions. The knockdown (KD) efficiency was validated by Western blot. The siRNA sequences are listed in Supplementary Table S1.

For stable GSTP1 overexpression (OE), human GSTP1 gene OE lentivirus was purchased from Beijing Tsingke Biotech Co., Ltd. (TSINGKE, China). The transfected A2780 cells were selected in culture media containing puromycin (2.5 μg/mL) for 1–2 weeks, and then positive infected cells were sorted for subsequent experiments. Puromycin was purchased from Beyotime, China.

2.4. Generation of KO cell

ATG5 was knocked out in A2780 cells using the CRISPR−Cas9 system. The guide RNA sequences for target were as follows: 5′-AAGAAAAAGCUGUAAGAACU-3′, 5′-AUCAGGAUGAGAUAACUGAA-3'. RNP complexes are prepared in a ratio of 5:1∼10:1 (sgRNA: Cas9). Nuclear transfection of Engs were performed with an electroporation instrument using the Ronsar and Thermofichenion transfection systems. Finally, single-cell sorting and expansion were completed by the DispenCell Single-Cell Dispenser of Molecular Device, and the monoclonal cells were screened for clear KO genotype (100 % KO editing) and cell lines with good viability (Supplementary Table S2).

2.5. Cell proliferation assay

The BeyoClick™ EdU Cell Proliferation Kit with Alexa Fluor 594 (Beyotime, China) was used to evaluate the proliferation of A2780 and SKOV3 cells. Cells were seeded in a 96-well plate at a density of 3.0×10^3 cells per well and exposed to rhCOLIII and human placental collagen types I and III for 48 h and the above kit was used to assess cell proliferation. In addition, chloroquine (autophagy inhibitor) and rapamycin (autophagy activator) were applied to examine the effects of rhCOLIII on autophagy inhibition.

2.6. Transwell assay

In the upper chamber, 50,000 cells per well were seeded, and rhCOLIII (8 mg/ml) dissolved in the medium was added to the lower chamber. After culturing for 48 h, the chambers were removed, fixed with paraformaldehyde (PFA, Beyotime, China) for 15 min and the invading cells were stained with 0.05 % crystal violet at room temperature and fixed with 4 % PFA for 15 min. The migrated cells were photographed by microscope (Nikon, Japan) and the number was counted.

2.7. Cell migration determination by scratch testing

A scratch test was performed to evaluate cell migration. OC cell lines A2780 or SKOV3, 1×10^6 cells per well, were respectively seeded on 6-well plates and cultured overnight to cover the entire bottom surface of the plate. A 100ul pipette tip was then used to scratch a vertical cross-hair on the bottom of the well plate by leaning against a sterile ruler. The cells were washed with phosphate buffered saline (PBS) three times to remove floating cells, and rhCOLIII (8 mg/ml), dissolved in serum-free medium, was added to each group, followed by incubation in a 37 °C incubator with 5 % CO_2. Finally, cell numbers in the scratched area were recorded using an inverted microscope (Nikon, Japan) at 0 h and 24 h.

2.8. Colony formation assay

The OC cell lines A2780 and SKOV3 were seeded in 6-well plates (200 cells per well), and rhCOLIII at a concentration of 8 mg/ml was added to each group. After incubation for 14 days, cells were stained with 0.1 % crystal violet after fixation with 4 % PFA for 15 min. Finally, the number of colonies formed was counted.

2.9. Flow cytometry

A2780 cells and SKOV3 cells (5×10^5 cells/well) were respectively seeded in 6-well plates for cell culture and adherence overnight. The cells were treated with different concentrations of rhCOLIII (1, 2, 4, and 8 mg/ml). A standard growth medium was used as negative control. After incubation for 48 h, adherent cells and stained. Annexin V-FITC apoptosis detection kit (Beyotime, China) and PI solution (Beyotime, China) were used, according to the manufacturer's instructions, to detect cell apoptosis and the cell cycle, respectively. Finally, cells were detected by flow cytometer (CytoFLEX, Beckman Coulter, USA) and the data were analyzed by Flowjo (TreeStar, USA).

2.10. Western blot assay

Cellular proteins were extracted using radioimmunoprecipitation assay (RIPA) buffer (Beyotime, China) with 1 % protease and 1 % phosphatase inhibitors (Beyotime, China), then compacted using ultrasound. Total protein concentration was then measured by a bicinchoninic acid (BCA) protein assay kit (Beyotime, China) according to the instructions. A quarter of the total volume of sodium dodecyl sulfate-polyacrylamide (SDS-PAGE) protein loading buffer, was then added, mixed and boiled for 5 min. Future PAGE™ 10 % 15 Wells (Boyi Biotech, China) gel electrophoresis was used to separate proteins, 0.45 μm Polyvinylidene Fluoride (PVDF) membranes (Merck Millipore, USA) to transfer proteins, and 5 % BSA to block the membranes. Membranes were then incubated overnight with a primary rabbit anti-MHC-I (1:1000, bs-7335 R, Bioss, Chain); anti-LC3 (1:1000, D3U4C, CST, US); anti-NBR1 (1:1000, E6Q3F, CST, US); anti-ATG3 (1:1000, 10181-2-AP, Proteinch, Chain); anti-ATG5 (1:1000, 111262-2-AP, Proteinch, Chain); anti-P62 (1:1000, 18420-1-AP, Proteinch, Chain); anti-GSTP1 (1:1000, 15902-1-AP, Proteinch, Chain), and then with a secondary goat anti-rabbit/mouse IgG antibody (bs-40295G-HRP, Bioss, China) for 0.5 h at room temperature. Finally, an enhanced chemiluminescence kit (Millipore, Burlington, MA, USA) was used to visualize the membrane signals which were analyzed with the software Image Lab 6.0 (Bio-Rad Lab., Hercules, CA, USA).

2.11. Co-immunoprecipitation (Co-IP)

The universal IP/Co-IP Toolkit Abbkine, China was used for Co-IP following the instructions. The cells were lysed with pre-cooled RIPA lysis solution and centrifuged at 4 °C and 12,000 g for 10 min, with the supernatant transferred to new centrifuge tubes. Anti-NBR1(1:1000), anti-MHC-I (1:1000), or IgG antibodies, were added to the lysates and the antigen–antibody mixtures were slowly shaken at 4 °C overnight. 20 μL Protein A/G agarose beads (Abbkine, China) were then added to capture the antigen–antibody complexes and slowly shaken at 4 °C overnight. The agarose bead-antigen-antibody complexes were harvested after washing 3 times. The samples were boiled for 5 min and then subjected to electrophoresis, with the protein expression assessed as for western blot as described above.

2.12. Ad-mCherry-GFP-LC3 transfection

To track the autophagy flux, SKOV3 and A2780 cells were stably infected with Ad-mCherry-GFP-LC3 (Genepharma, China). 5×10^5 cells per well were seeded in 6-well plates and transduced with Ad-mCherry-GFP-LC3 for 24 h. Autophagic capacity was observed and measured by counting yellow and red signal dots inside the cells using a confocal microscope (Nikon Eclipse Ti, Japan).

2.13. Immunofluorescence Confocal Microscopy

Recent studies have revealed that autophagy can selectively degrade target molecules using autophagy cargo receptor proteins to up-regulate immunity, and the major histocompatibility complex class I (MHC-I) has shown a close relationship with the autophagy cargo receptor neighbor of BRCA1 gene 1 (NBR1). Immunofluorescence Confocal Microscopy was performed to examine this relationship in the OC cell line A2780. After exposure to rhCOLIII for 48 h, cells were fixed with 4 % PFA for 10 min and permeabilized with 0.1 % Saponin. 5 % normal goat serum was used to block samples for 30min at room temperature followed by incubation with the primary antibodies anti-NBR1 (1:100) and anti-MHC-1 (1:100) overnight at 4 °C. Incubation with fluorescent secondary antibodies and then 4′,6-diamidino-2-phenylindole (DAPI) solution (Beyotime, China) followed, in the dark at 37 °C, to stain nucleic acids. Cells were observed by confocal laser scanning microscopy (Nikon Eclipse Ti, Japan).

2.14. Biotin labeling and tracking of rhCOLIII

Biotin Quick Labeling Kit (Frdbbio, Wuhan, Chain) was used to label rhCOLIII. Biotin was dissolved in dimethyl sulfoxide (DMSO, Solarbio, China) to a final concentration of 10 mM. Labeling buffer was used to dissolve rhCOLIII (8 mg/ml), Biotin was added and incubated at 37 °C, protected from light for 30 min, placed in an ultrafiltration tube, then centrifuged at 12,000×*g* for 10 min, and this step was repeated 3 times to collect biotin-labeled rhCOLIII. A2780 cells were exposed to Biotin-labeled rhCOLIII for 2, 4, 6, 12, and 24 h, tracking the distribution of labeled rhCOLIII. After fixation with PFA and blocking with 5 % normal goat serum for 30 min, cells were incubated with primary antibodies anti-GSTP1 1:100, overnight at 4 °C. Fluorescent secondary antibodies Rhodamine B isothiocyanate (RBITC) and Fluorescein 5-isothiocyanate (FITC) were added at 37 °C for 1 h in darkness. DAPI solution was added to stain nucleic acids and samples were observed by confocal laser scanning microscopy.

2.15. Animal models: Establishment and treatments

All animal experiments were performed in compliance with the guidelines of the Institutional Animal Care and Use Committee of Chongqing Medical University. Female nude mice (4 weeks old) were purchased from the Experimental Animal Center of Chongqing Medical University for tumorigenicity investigation purposes. As previously described, A2780 cells (5×10^6) suspended in normal saline were injected subcutaneously, and the tumors were allowed to reach a 100 mm^3 volume, following which the animals were randomly divided into two groups, the control group and the rhCOLIII group, with five animals per group. Then, to investigate the anti-tumor efficacy of rhCOLIII *in vivo*, 100ul sterilized PBS solution and 100ul rhCOLIII solution (8 mg/

ml) were respectively injected subcutaneously around the tumor in the control group and the rhCOLIII group every 3 days. The dosage of rhCOLIII in each mouse was 0.8 mg. The tumor volumes and mouse weights were measured every 3 days. 12 days after treatment, the mice were sacrificed, the tumors were removed, and then fixed and paraffin-embedded for tissue staining.

Female BALB/C mice (6 weeks old) were purchased from Chongqing Enswell Biotechnology Co., Ltd. and raised in a specific pathogen free (SPF) environment. Mouse OC cell ID8 cells (5×10^6) were inoculated on the left side of the axillary area of mice. Approximately 6 days later, when tumors were palpable, the mice were separated into the control group and the rhCOLIII group with an even distribution of tumor volumes. The control group and the rhCOLIII group were respectively injected with the same volume of PBS and dissolved rhCOLIII by intraperitoneal injection every 3 days, tumor volumes and body weights were measured at the same time. The volume of PBS and rhCOLIII was 100ul per mouse, and the concentration of rhCOLIII was 8 mg/ml. After treatment for 18 days, we removed the tumors and measured their volumes and weights. Additionally, to extract immune cells ($CD3^+$ T cells, $CD4^+$ T cells, $CD8^+$ T cells) from peripheral venous blood, BALB/C mice (5 per group) were anesthetized, and the eyeballs were removed. For surface labeling, immune cells were suspended in a staining buffer and incubated for 15 min at room temperature in the dark with the following fluorophore-conjugated anti-mouse monoclonal antibodies (mAbs) (BioLegend): phycoerythrin (PE)-conjugated anti-CD3, fluorescein isothiocyanate (FITC)-conjugated anti-CD4, PE-conjugated anti-CD8. The pellet was finally resuspended in 200ul of PBS, subjected to flow cytometry (Beckman, America) and analyzed using FlowJo and GraphPad Prism 7 software.

To further verify the biosafety of rhCOLIII *in vivo*, 10 female nude mice and 10 BALB/C around 5 weeks old were randomly divided into the control and the rhCOLIII group, with 5 mice, of each type, in a group. After 6 days, nude mice were injected subcutaneously with an equal volume of PBS and rhCOLIII, and BALB/C mice were given intraperitoneal injection with an equal volume of PBS and rhCOLIII. The injection volume was 100ul, the concentration of rhCOLIII was 8 mg/ml, and the mice were injected every 3 days and their body weights were measured. After treatment for 12 days, the main organs (heart, liver, lung, kidney, spleen) of mice were embedded in paraffin, and H&E stain to evaluate safety. In addition, we tested the liver and kidney function of the two groups by biochemistry of the peripheral blood of the BALB/C mice.

2.16. Immunohistochemistry and specific stains

Subcutaneous tumors in nude mice were surgically dissected and the excised tissue was preserved and fixed with 4 % PFA. Tissue sections were cut at 5 μm and stained with hematein-erythrosin-Safran for routine histologic analysis and specific stains using the relevant kit, including Masson trichrome using a Masson stain kit (Sewell, Wuhan), Sirius red stain (MEIMIAN, Chain) and TUNEL assay by Abcam TUNEL Assay Kit-HRP-DAB kit (Roche, Shanghai).

The routine immunohistochemistry steps included; firstly, placing the paraffin sections in a 60 °C oven, warming for 2 h, then removal and dehydration with xylene and alcohol; secondly, citric acid antigen retrieval buffer was used for antigen retrieval; and thirdly, endogenous peroxidase was blocked with 3 % hydrogen peroxide for 10 min at room temperature in the dark. The fourth step was addition of 5 % goat serum for blocking and the fifth step was addition of primary antibodies anti-NBR1 (1:300), anti-MHC-1 (1:250), anti-P62 (1:250), and anti-LC3 (1:250) with incubation overnight at 4 °C. The sixth step involved dropwise addition of secondary antibody and incubation at room temperature for 15 min. Finally, DAB staining was performed and at least three fields of view were randomly selected for photography using a Nikon instrument with analysis by ImageJ software.

Human ovarian tissue microarrays (ZLOVA961) were purchased from Shanghai Zhuolibiotech Company Co., Ltd. (Shanghai, China), and GSTP1 expression was evaluated using the automated VIS DIA VisioMorph System (Visiopharm®, Hoersholm, Denmark). Relevant clinical and pathological information was obtained from the array manufacturer.

2.17. Immunofluorescent staining

Paraffin sections were deparaffinized and dehydrated. Next, the sections were blocked with 10 % goat serum for 1 h at 37 °C after antigen retrieval. The sections were incubated with primary antibodies, including anti-CD3 (1:200, Abcam, US), anti-CD4 (1:200, Abcam, US), anti-CD8 (1:200, Abcam, US), MHC-1(1:100, Proteinch, China) and LC3 (1:100, Santa, US) overnight at 4 °C. After being washed three times, the sections were incubated with fluorescent-conjugated secondary antibodies for 1 h at 37 °C, and then 4′6-diamidino-2-phenylindole solution was used for nuclear staining. The sections were observed under a fluorescence microscope at 200 × magnification (Nikon Corporation, Tokyo, Japan).

2.18. Transmission electron microscopy (TEM)

A2780 cells were trypsinized and pelleted. Cells were then fixed with 2 % glutaraldehyde and 1 % osmium tetroxide, rinsed in 100 mM sodium phosphate buffer (pH 7.2), dehydrated in ethanol before embedding and preparing ultrathin sections. Ultrathin sections of A2780 cells were collected on formvar-coated grids and stained with 10 % uranyl acetate and 1 % lead citrate and then examined with an H600 Transmission Electron Microscope (Hitachi, Japan) operated at 80 KV.

2.19. Second harmonic generation (SHG) microscopy

Sections were taken from formalin-fixed paraffin-embedded tumors for SHG imaging, and slides were analyzed using the Olympus laser scanning FV1200 MPE multiphoton microscope (Olympus, Japan) with a 25Xw/1.05XLPLN MP lens. Excitation was achieved at 860 nm and a second harmonic signal was detected at 430 nm.

2.20. Quantification and testing of RNA-seq data and proteomics

Single-cell RNA-sequencing (scRNA-Seq) and proteomics were used to analyze mRNA transcripts and protein for differential expression between rhCOLIII treated and control A2780 cells. Protein and RNA samples were collected from cell lysates, three pairs each for experimental and control samples, and the prepared sample were sent to Novogene Co., Ltd (Beijing, China) for testing. Proteomics determination was divided into the following steps: total protein extraction, protein quality testing, peptide labelling, separation of fractions, LC-MS/MS analysis, and data analysis. RNA-seq testing was followed by RNA qualification and data analysis, including gene expression level, differential expression analysis, enrichment analysis of differentially expressed genes, Gene Set Enrichment Analysis (GSEA), SNP, AS, PPI, and fusion analysis and Weighted correlation network analysis (WGCNA).

2.21. Edman degradation

Edman degradation was performed to detect the N-terminal sequencing of rhCOLIII, by transferring the rhCOLIII to the PVDF membrane, placing the sheared PVDF membrane in the reactor, and testing it by software PPSQ Automated Protein Peptide Sequencer (SHIMADZU, China). The analysis was performed on Software PPSQ Analysis/Labsolutions.

2.22. Liquid chromatograph mass spectrometer (LC-MS/MS)

High-resolution mass spectrometry (Waters, US) and ultra-

performance liquid chromatography (Waters, US) were used to detect the C-terminal sequencing of rhCOLIII. RhCOLIII was dissolved with 150 mM Tris (pH 7.8), Lys-C was added at 37 °C for 30min. Then using ultra-high performance liquid chromatography separation and mass spectrometry analysis after the termination of reaction. Seetings included analysis duration: 45 min, detection mode: positiveIon (MSE), precursor ion scanning range: 300–2000m/z. Data were evaluated using software using UNIFI (Waters, US) software.

2.23. The cancer genome atlas (TCGA) database

The potential role of GSTP1 in ovarian cancer was validated by examining the TCGA (http://www.cbioportal.org) and GEPIA (http://gepia.cancer-pku.cn/) databases.

2.24. Statistical analysis

All experiments were repeated at least three times. All data were analyzed by GraphPad Prism 9.0 (GraphPad Software Inc., US) software and presented as mean and standard deviation. The statistical methods used included one-way analysis of variance (ANOVA) and student's t-test. We defined $P < 0.05$ as an indication of a significant difference (*$P < 0.05$, **$P < 0.01$).

3. Results

3.1. rhCOLIII, a special biomaterial, inhibited the proliferation, migration, and invasion of A2780 and SKOV3 cells, and induced apoptosis and cell-cycle arrest

rhCOLIII, a new biosynthetic medical material with a stable triple helix structure, was proved by Fourier analysis (Figure S1 (B)), screening of the amino acid sequence at positions 483–512 in the core functional region of human type III collagen and assembling in tandem 16 times (Fig. 1 (A)), with a total of 480 amino acids and a molecular weight of about 45 kDa (Figure S1 (D)). The results of Edman degradation and LC-MS/MS for the detection of N-terminal and C-terminal sequences of rhCOLIII were GERGAPGFRGPAGPN and GIPGEKGPAGERGAP, respectively (Figure S1 (A)). The microstructure and morphology of rhColIII were observed by SEM (Hitachi, Japan). We discovered flaky and flexible fibers intricately woven into a network structure with uniformly distributed porosity and neat arrangement, featuring pore diameters ranging from 10 to 20 μm (Figure S1 (C)). In addition, we further assessed the biosafety of rhCOLIII *in vivo*. Liver and kidney functions of female BALB/C mice were evaluated. No significant differences were observed between the control group and the rhCOLIII treatment group (Supplementary Table S3). However, the increase in peripheral blood T lymphocytes (CD3, CD4, and CD8 T cells) by flow cytometry indicated that rhCOLIII enhanced T cell immunity in normal BALB/C mice (Figure S3 (A)). Additionally, HE staining of heart, liver, spleen, lung, and kidney tissues showed no significant differences between the control group and the rhCOLIII treatment group in female BALB/C mice and nude mice (Figure S3 (C)). Furthermore, the body weights of female BALB/C mice and nude mice between the two groups also showed no great difference (Figure S3(B)). These characteristics strongly supported the high biological activity, water solubility and biosafety of rhCOLIII.

The EdU and colony formation assays were performed to investigate the effect of rhCOLIII on the growth of the OC cell lines A2780 (and SKOV3). The results showed that rhCOLIII had a dose-dependent effect on the growth of OC cells, with the most statistically significant effect at a concentration of 8 mg/ml (Fig. 1(B and C), Figure S2 (A)). The concentration of 8 mg/ml rhCOLIII was chosen by CCK-8 assay (Fig. 1 (D)) and used for follow-up experiments. However, EdU assay showed that rhCOLIII (8 mg/ml) had no significant inhibitory effect on the growth of normal epithelial ovarian cells ISOE and HOSEpiC (Fig. 1 (E)). Compared with the control group, rhCOLIII significantly inhibited A2780 cell proliferation, while human placental collagen type I promoted A2780 cell proliferation, although human placental collagen type III had no significant effect (Figure S1 (E)). The scratch test results showed that rhCOLIII (8 mg/ml), significantly inhibited migration of OC cells within 24 h (Fig. 1 (F)). rhCOLIII (8 mg/ml), significantly reduced the invasion of OC cells (Fig. 1 (G)). Additionally, rhCOLIII, at a concentration of 8 mg/ml, significantly promoted apoptosis of the OC cell lines A2780 and SKOV3 (Fig. 1(H)) and increased the proportion of OC cell lines A2780 and SKOV3 in the G1 phase (Figure S2 (B)).

3.2. rhCOLIII inhibited autophagy in OC cells

To investigate whether rhCOLIII affected cell autophagy, we first quantified the levels of autophagy-related proteins, LC3, P62, ATG3, ATG5 and NBR1. Basal levels of ATG3, ATG5, LC3 and NBR1 were significantly decreased, and the level of P62 was significantly increased by rhCOLIII, the effect varies with the concentration gradient of rhCOLIII (Fig. 2 (A)). In addition, to monitor autophagic flux, Ad-mCherry-GFP-LC3 was used to infect OC cells and rhCOLIII significantly decreased LC3 dot accumulation and inhibited OC cells autophagy (Fig. 2 (B)). Furthermore, we also observed a significant reduction in the number of autophagosomes in A2780 cells treated with rhCOLIII by TEM (Fig. 2 (C)). Previous studies demonstrated that the precise regulation of autophagy in cancer cells was an effective anticancer approach [19]. In order to explore the relationship between the anti-tumor function of rhCOLIII and autophagy regulation, we inhibited the autophagy pathway by knocking out (KO) ATG5 (Figure S2 (D)), a key autophagy gene, and adding the autophagy inducer, rapamycin, to promote the autophagy pathway. Our results showed that promoting autophagy significantly increased the proliferation of A2780 cells, but had no significant effect on SKOV3 cells. Additionally, the proliferation ratio in OCCs treated with rapamycin was significantly reduced after rhCOLIII treatment (Fig. 2 (E)). Furthermore, we observed the anti-proliferative effect of rhCOLIII on ATG5 KO cells was abrogated (Fig. 2 (D)). These findings strongly suggested that rhCOLIII suppressed OC proliferation via autophagy inhibition.

3.3. rhCOLIII inhibited the immune escape of OC cells by regulating autophagy

We conducted transcriptome sequencing to identify the differentially expressed genes before and after rhCOLIII treatment and found 1625 genes had been significantly up-regulated, including three MHC-1 related genes (Figure S2 (E)). Accumulating studies found that autophagy has great influence on the immune system of the cancer microenvironment, particularly the immune molecule MHC-1, which inhibited antigen presentation and assisted cancer cells to escape immunity [20]. Therefore, to explore the effect of autophagy on MHC-1 in OC, we measured the expression of MHC-1 when autophagy was respectively promoted and inhibited by rapamycin and chloroquine, the results of Western blot suggested that the expression of MHC-1 in OC cells treated with chloroquine was significantly enhanced (Fig. 3 (A)). We further evaluated the effects of rhCOLIII on the expression of MHC-1, demonstrating incremental increase of MHC-1 in A2780 cells treated with increasing concentrations of rhCOLIII (0, 2, 4, 8 mg/ml) (Fig. 3 (C)). Immunofluorescence also confirmed that rhCOLIII and chloroquine promoted the expression of MHC-1 in SKOV3 and A2780 cells (Fig. 3 (B)). These findings demonstrated autophagy inhibition could prevent immune escape *in vitro*. Subsequently, to identify the key autophagy protein in regulating MHC-1 expression, we silenced the autophagy related proteins ATG3, ATG5, NBR1 and P62 (Figure S2 (C)), and found that MHC-1 was upregulated most significantly in the siNBR1 group (Fig. 3 (D)). In addition, Co-IP and immunofluorescence revealed that NBR1 and MHC-I may interact and co-localize (Fig. 3(E and F)). However, the effects of rhCOLIII on the proteins MHC-1 and NBR1were

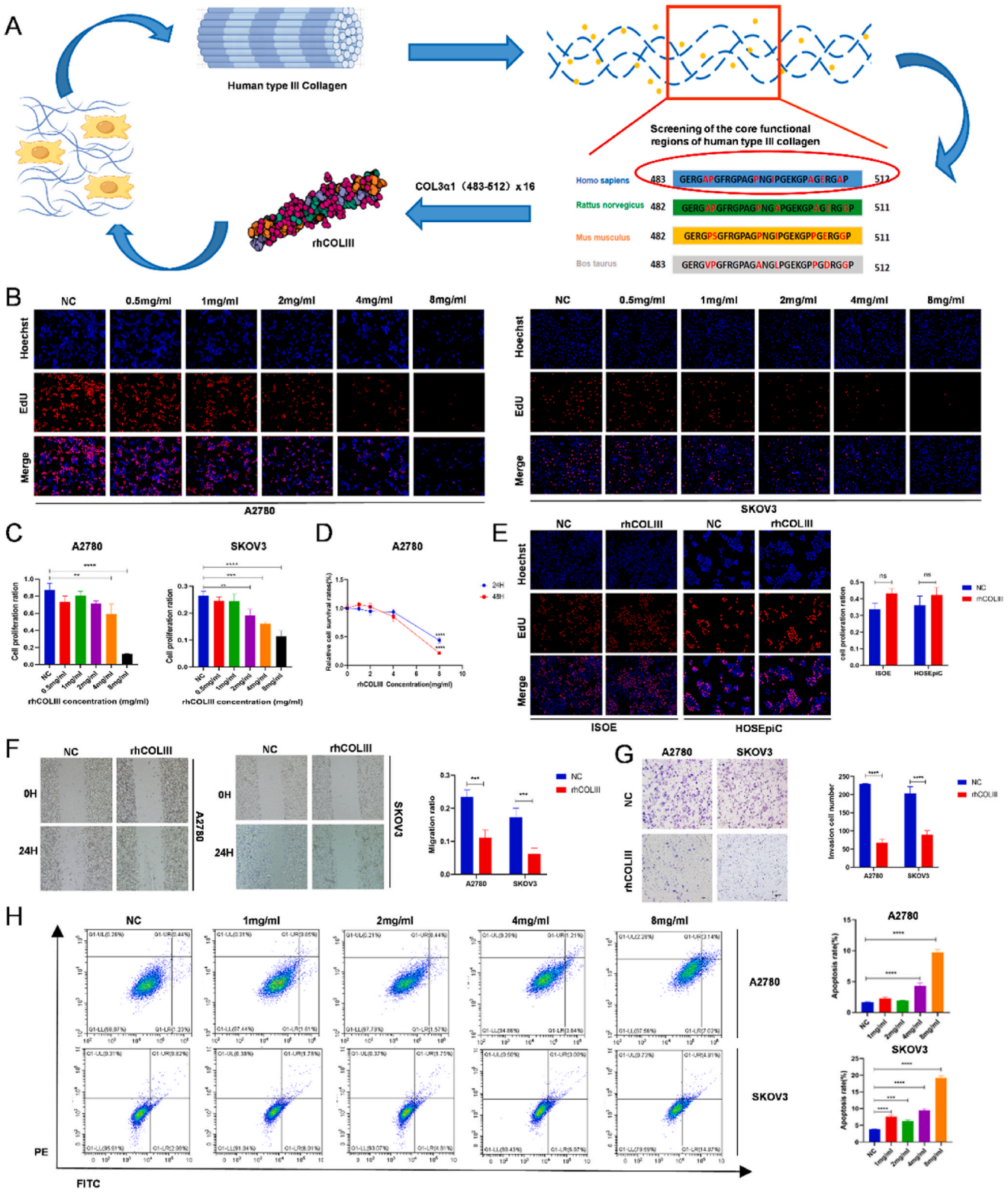

Fig. 1. rhCOLIII inhibited the proliferation, migration, and invasion of A2780 and SKOV3 cells, and induced apoptosis and cell-cycle arrest. **(A)** Schematic diagram of the screening process of the core functional region of human type III collagen. **(B)** The EdU cell proliferation assay of A2780 and SKOV3 cells treated with different concentrations of rhCOLIII (0, 0.5, 1, 2, 4, and 8 mg/ml). Scale bar = 100 μm. **(C)** The statistical results of EdU cell proliferation assay of A2780 and SKOV3 cells after treatment with different concentrations of rhCOLIII (0, 0.5, 1, 2, 4, and 8 mg/ml). **(D)** Survival of A2780 cells treated with different concentrations of rhCOLIII as determined by CCK-8 (Cell Counting Kit-8) assay. **(E)** The proliferation ratios of ISOE and HOSEpiC cells after treatment with rhCOLIII, were determined by EdU assay. Scale bar = 100 μm. **(F)**Representative images of wound healing assays are shown; the migration capability of A2780 and SKOV3 cells after treatment with rhCOLIII. Scale bar = 200 μm. **(G)** Representative images of transwell assays are shown; the invasion ability of A2780 and SKOV3 cells after treatment with rhCOLIII. Scale bar = 10 μm. **(H)** rhCOLIII induced apoptosis in A2780 and SKOV3 cells. Apoptosis was detected by Annexin V-FITC and propidium iodide (PI) staining. Data are presented as mean ± SD of three independent experiments. The symbols *, **, and *** show $P < 0.05$, 0.01, and 0.001 versus the control group.

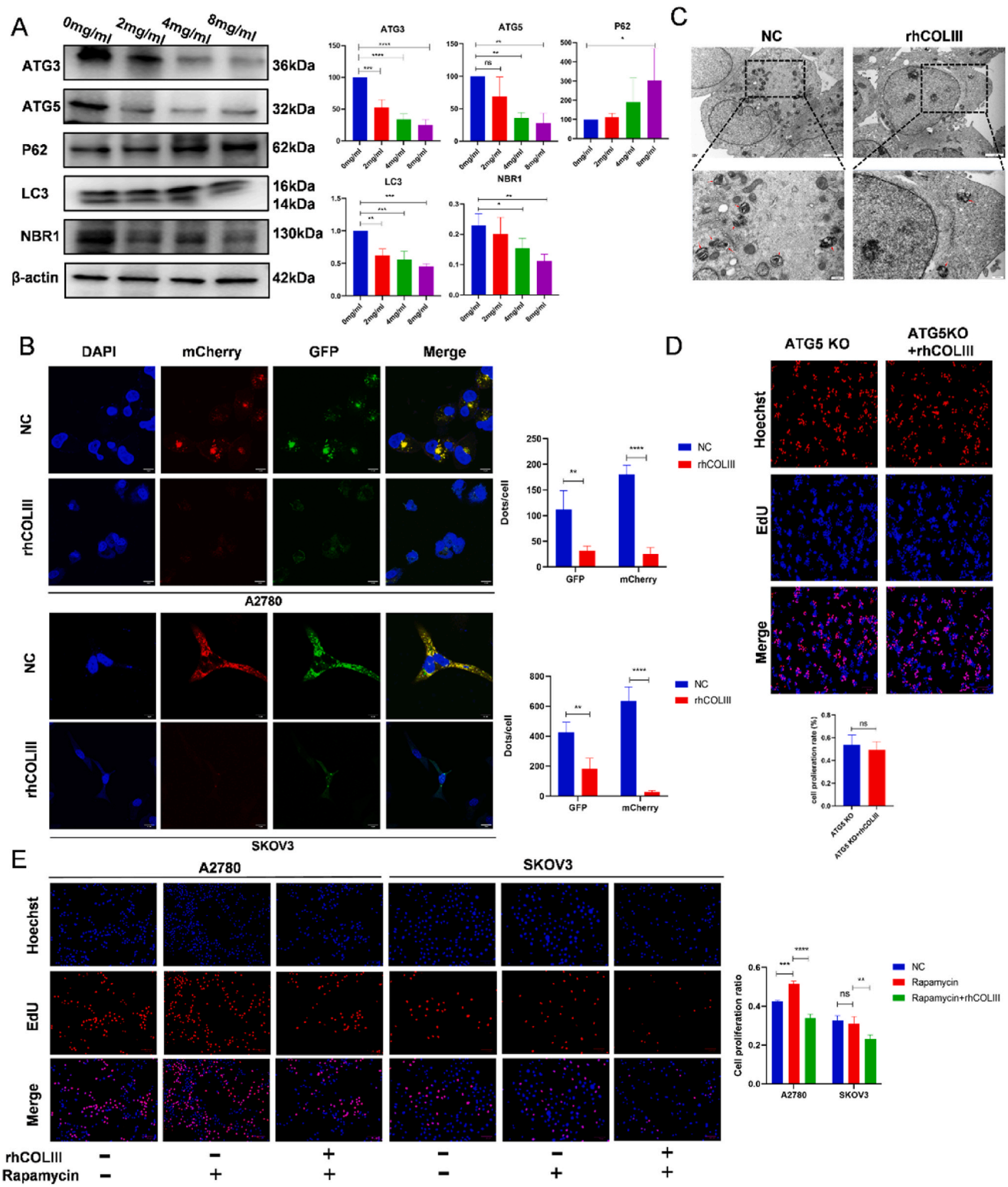

Fig. 2. rhCOLIII inhibited autophagy in OC cells. **(A)** Western blot analysis of autophagy-related proteins (ATG3, ATG5, P62, LC3, NBR1) in A2780 cells treated with different concentrations of rhCOLIII (0, 2, 4, and 8 mg/ml). β-actin was the loading control. **(B)** Autophagy flux in A2780 and SKOV3 cells transfected with mCherry-GFP-LC3, detected by confocal microscopy, with quantification of the LC3 dots in each cell. Scale bar = 10 μm. **(C)** The number and morphology of autophagosomes in A2780 cells observed by TEM, the red arrow points to the autophagosome. **(D)** The EdU assay was used to detect the proliferation of ATG5 KO A2780 cells and ATG5 KO A2780 cells with rhCOLIII treatment, Scale bar = 100 μm. **(E)** The proliferation ratios of A2780 and SKOV3 cells after treatment with rapamycin and rapamycin combined with rhCOLIII detected by EdU assay. Scale bar = 100 μm. Data are presented as mean ± SD of three independent experiments. The symbols *, **, and *** show $P < 0.05$, 0.01, and 0.001 versus the control group. (For interpretation of the references to colour in this figure legend, the reader is referred to the Web version of this article.)

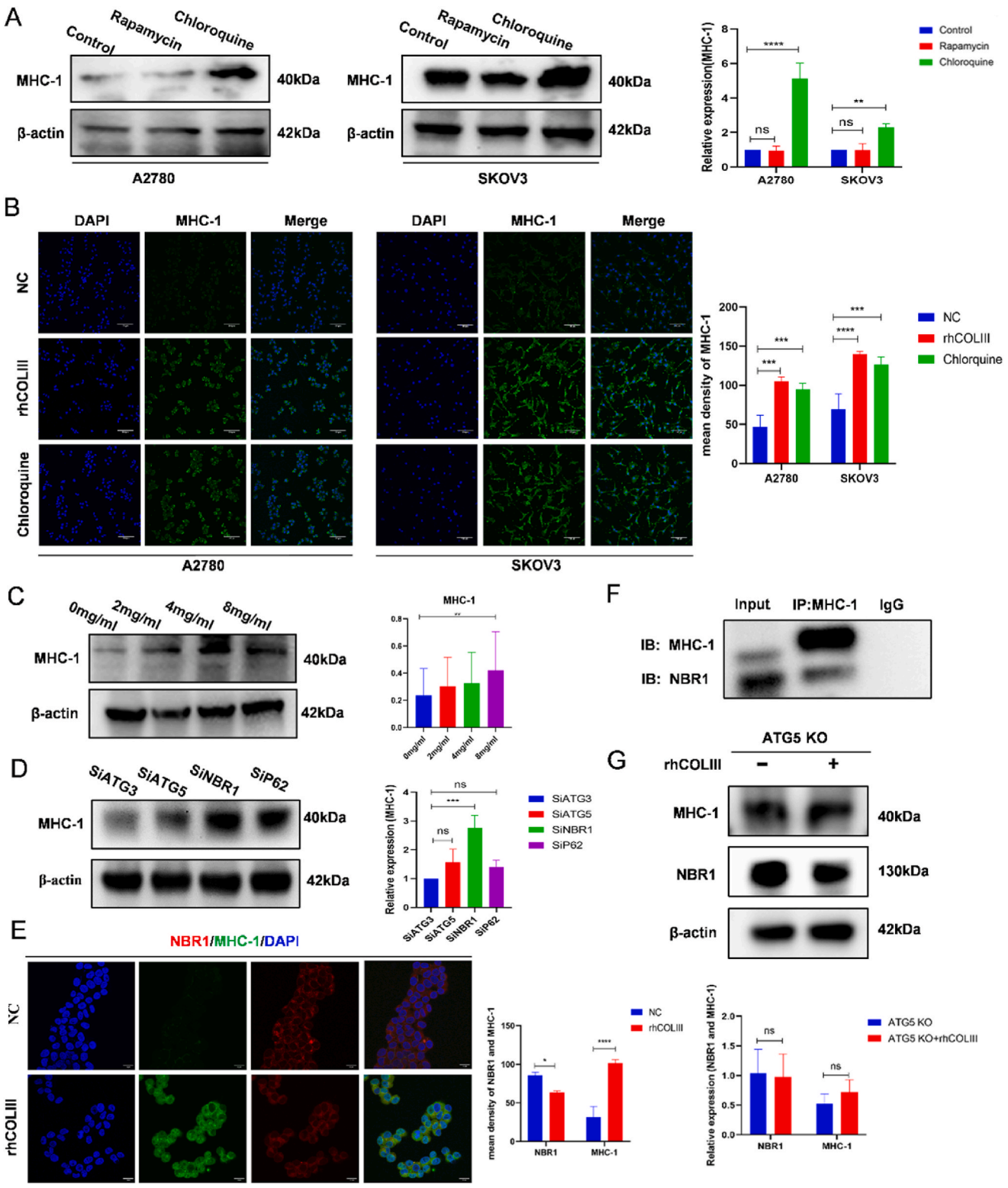

Fig. 3. rhCOLIII inhibited the immune escape of OCs by regulating autophagy. **(A)** Western blot analysis of MHC-1 expression in A2780 and SKOV3 cells treated with rapamycin and chloroquine. **(B)** Representative images of immunofluorescence of MHC-1 (green) in OCCs treated with rhCOLIII and chloroquine respectively. Scale bar = 10 μm. **(C)** Western blot analysis of MHC-1 expression in A2780 cells treated with different concentrations of rhCOLIII (0, 2, 4, and 8 mg/ml). **(D)** Western blot analysis of MHC-1 expression in ATG3 KD A2780 cells, ATG5 KD A2780 cells, NBR1 KD A2780 cells and P62 KD A2780 cells. **(E)** Localization of MHC-I (red) relative to GFP-NBR1 (green) in A2780 cells by confocal microscopy. Scale bar = 10 μm. **(F)** Co-IP was applied to confirm the relationship between NBR1 and MHC-1. **(G)** Western blot analysis of MHC-1 and NBR1 expression in ATG5 KO A2780 cells and ATG5 KO A2780 cells after rhCOLIII treatment. Data are presented as mean ± SD of three independent experiments. The symbols *, **, and *** show $P < 0.05$, 0.01, and 0.001 versus the control group. (For interpretation of the references to colour in this figure legend, the reader is referred to the Web version of this article.)

abrogated in ATG5 KO cells (Fig. 3 (G)). These findings indicated that rhCOLIII inhibited the immune escape via autophagy reduction.

3.4. rhCOLIII specifically inhibited autophagy and immune escape by regulation of GSTP1 expression

A heatmap of differentially expressed genes and proteins, by joint analysis of RNA-Seq and proteomics, comparing control and rhCOLIII treatment groups was constructed (Fig. 4 (A)). KEGG pathway analysis of downregulated genes showed that they were associated with autophagy-related pathways in A2780 cells treated with rhCOLIII (Fig. 4 (B)). The TCGA database also showed high expression of the GSTP1 gene in OC, and this gene was significantly correlated with collagen formation and the classical autophagy, PI3K-AKT-mTOR, pathway. In addition, the TCGA database excavation suggested that GSTP1 may be related to $CD8^+$ T cells and assessing the immune score (Fig. 4 (C)). Tissue microarray staining for GSTP1, and also the GEPIA2 database, showed that GSTP1 expression in OC was significantly higher than in the normal population Fig. 4(D and E). In addition, we found that the expression of GSTP1 was downregulated with increase of rhCOLIII by Western blot (Fig. 4 (F)). In order to further investigate the correlation between rhCOLIII and the GSTP1 protein, we used biotin-labeled rhCOLIII to observe its distribution in A2780 cells at different times (2, 4, 6, 12, and 24 h) by confocal microscopy, rhCOLIII may be colocalization with the GSTP1 protein. (Fig. 4 (H)). In addition, TEM was used to examine the subcellular structure of A2780 cells treated with rhCOLIII at different time points (0, 6, 12, and 24 h), demonstrating that rhCOLIII may enter the cells and exert biological activity (Fig. 4 (I)).

To further verify rhCOLIII inhibited autophagy and exerted antitumor function through GSTP1, we respectively observed the effects of GSTP1 KD and OE (Fig. 4 (G)) on OC cells proliferation, migration, invasion and autophagy. In addition, the above phenotypic changes were detected after rhCOLIII treatment of the GSTP1 KD and OE OC cells. Our results showed that inhibition of the proliferation (Fig. 5 (A)), migration (Figure S3 (D)) and invasion (Figure S3 (F)) of A2780 cells was significantly greater in GSTP1 KD cells, compared to the SiNC group, and significantly lower in GSTP1 OE cells (Fig. 5 (B), Figures S3(E, G)), compared to the GSTP1-OE NC group. To further verify that rhCOLIII inhibited autophagy and improved immunity through GSTP1, we examined changes in autophagy and MHC-1 immune molecules on GSTP1 KD and OE OC cell lines. Immunofluorescence and western blot showed that NBR1 expression was significantly decreased, MHC-1 expression was significantly increased on the GSTP1 KD cells, compared to the SiNC group (Fig. 5 (C, D, E, F)). However, on the GSTP1 OE cells, NBR1 expression was significantly greater, MHC-1 expression was significantly lower compared to the GSTP1-OE NC group (Fig. 5 (G, H, I, J)). Additionally, compared to the SiNC group, autophagy-related proteins LC3 and autophagic flow were significantly decreased, and P62 was significantly increased on the GSTP1 KD cells (Fig. 6 (A, B, C, D)). In the GSTP1 OE cells, LC3 and autophagic flow were significantly greater than in the GSTP1-OE NC group, while the expression of P62 was significantly lower (Fig. 6 (E, F, G, H)). However, compared to the effects of rhCOLIII on A2780 cells without KD or OE, the effects of rhCOLIII on GSTP1 KD cells were abrogated, and the effects of rhCOLIII on the GSTP1 OE cells were weakened, which further supported GSTP1 mediation of the effects of rhCOLIII on OC.

3.5. rhCOLIII inhibited tumor growth, positively regulated immunity and remodeled extracellular matrix (ECM) in vivo

In a model of subcutaneous tumorigenesis in nude mice, the average volume and weight of tumors in the rhCOLIII group were significantly lower than that in the control group (Fig. 7(A and B)), while the proportion of apoptotic cells by TUNEL staining was significantly higher in the rhCOLIII group (Fig. 7 (D)). Furthermore, IHC analysis revealed that the expression of P62 and MHC-1 was significantly greater in the rhCOLIII group, while NBR1 and LC3 were significantly lower, compared to the control group (Fig. 7 (C)). Considering the function of rhCOLIII in regulation of ECM, we detected the content, the type and morphological structure of collagen *in vivo*. Masson and Sirius red staining of subcutaneous tumor tissues showed that the amount of collagen, especially the type III collage, was significantly higher in the rhCOLIII group (Fig. 7 (G)). The morphology of collagen, detected by SHG imaging, was curlier and more neatly arranged after rhCOLIII treatment in subcutaneous tumor tissues of mice, in contrast to the rigid and disordered collagen found in human OC tissue (Fig. 7 (F)). Changes in collagen morphology, quantity and proportion indicated that rhCOLIII cloud remodel TEM into a healthier ECM (Fig. 7 (E)).

The antitumor effect of rhCOLIII on implanted mouse OC ID8 cells in BALB/C mice was examined according to the dosing regimen shown in Fig. 8 (A) rhCOLIII significantly inhibited tumor growth, and reduced the volume of the tumors after 18 days of treatment, compared to the control group (Fig. 8 (B)). Immunofluorescence double-staining indicated that compared to the control group, LC3 was significantly downregulated, MHC-1 was significantly up-regulated in the rhCOLIII group (Fig. 8 (E)). Subsequetly, we performed multiplex immunofluorescence staining of CD3, CD4, CD8 in mice tumor tissues and demonstrated that rhCOLIII significantly increased the infiltration of immune T cells (Fig. 8 (D)). In addition, flow cytometry showed the same results that the expression of peripheral blood T lymphocytes (CD3, CD4, and CD8 T cells) in BALB/C mice models of OC increased significantly after rhCOLIII treatment (Fig. 8 (C)). These data strongly suggested that rhCOLIII induced protective antitumor immunity *in vivo*.

4. Discussion

OC is a leading cause of death in women, patients are often asymptomatic and diagnosed late in the disease course, with distant metastasis and malignant ascites. Although surgery combined with chemotherapy improves patient survival, nearly 80 % eventually relapse into chemoresistance resulting in a low five-year survival rate [21]. Unlike most solid tumors, OCCs disseminate by direct extension into the peritoneum with cell shedding, interacting with mesothelial cells lining the peritoneum, later invading the underlying basement membrane and spreading across the ECM forming metastatic implants [22,23]. Malignant cells closely interact with the surrounding ECM, resulting in its continuous remodeling. Collagen is the most abundant proteins in the ECM, with different subtypes, structure and proportion [24,25]. Research has demonstrated that collagen is a double-edged sword as regards tumor progression, closely related to the morphological structure, subtype and quantity of collagen [26–28]. In cancers, the normal ECM becomes highly dysregulated, rigid, and fibrotic, serving pro-tumorigenic roles [29]. Furthermore, type III collagen, one of the common subtypes, was reported to decrease in OC associated with an increased risk of intraperitoneal metastasis [9,30,31]. Therefore, targeting type III collagen is a potential, novel therapeutic strategy to regulate the ECM and cell-ECM interactions.

In our previous studies, rhCOLIII was shown to have broad properties as a biomedical material, including promoting the regeneration of atrophied vaginal epithelium, improving pelvic floor function, repairing UV-damaged skin, regulating endometrial inflammation and remodeling the immune microenvironment, as well as exerting significant antitumor effects in breast cancer [16–18,32,33]. Therefore, we aimed to further explore the function and mechanism of action of rhCOLIII on OC *in vitro and in vivo*. We demonstrated that rhCOLIII significantly inhibited proliferation, migration, invasion and promoted apoptosis of OCCs by regulating autophagy. Additionally, rhCOLIII could suppress immune escape via autophagy decrease. These functions of rhCOLIII were also confirmed by *in vivo* experiments, rhCOLIII could reduce the volume of subcutaneous tumors in nude mice and positively trigger immunity in BALB/C mice (Fig. 9).

To further explore the mechanisms rhCOLIII anti-tumor actions and

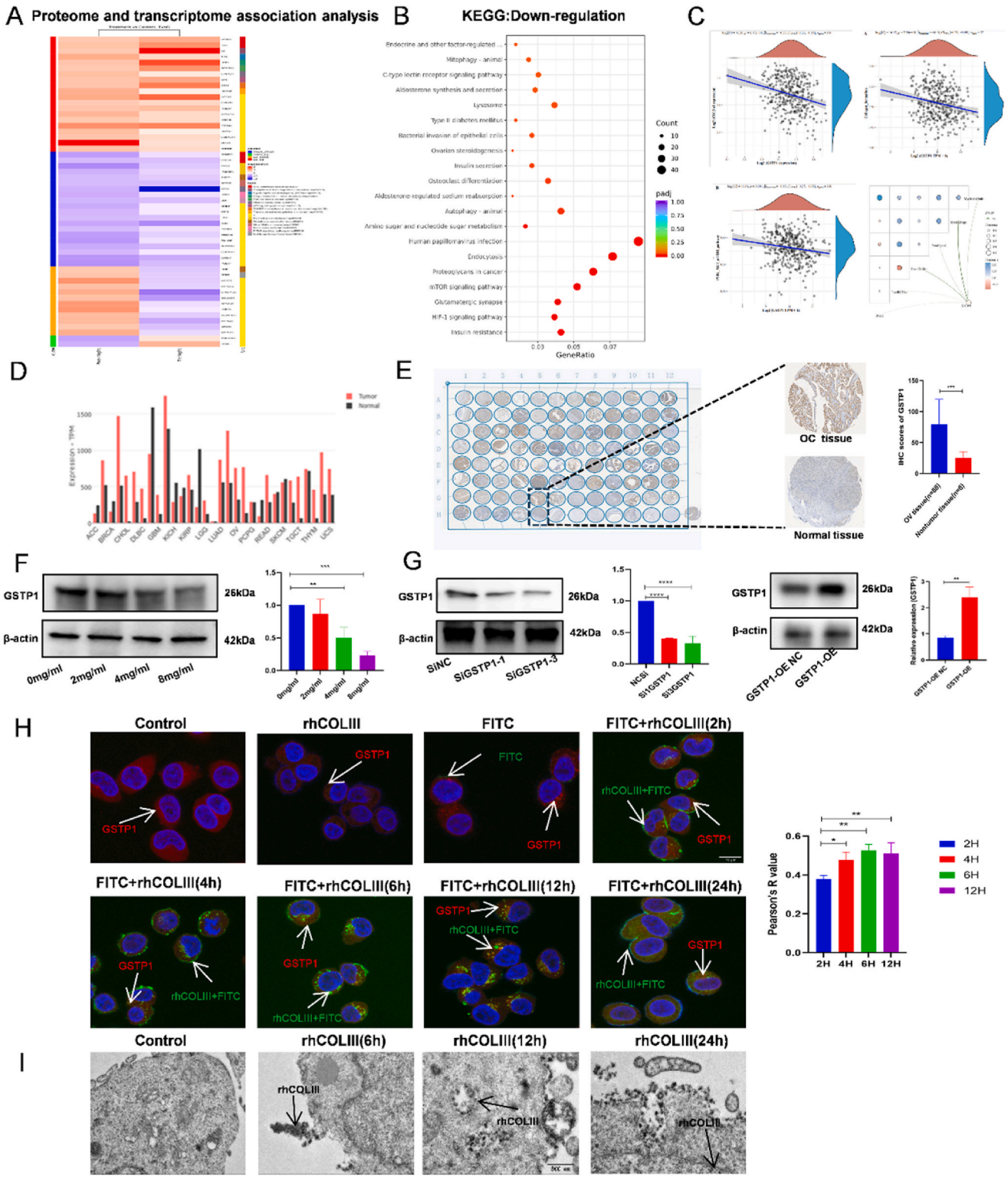

Fig. 4. rhCOLIII specifically inhibited autophagy and immune escape by regulating GSTP1 expression. **(A)** KEGG pathway analysis for proteome and transcriptome combined sequencing in A2780 cells with rhCOLIII treatment. **(B)** KEGG pathway analysis for down-regulated genes in A2780 cells treated with rhCOLIII. **(C)** Spearman correlation of GSTP1 with COL3A1 expression, collagen formation, and the PI3K-AKT-mTOR pathway in the TCGA database. The immune score of the gene GSTP1 in OC in the TCGA database. *P* values and Spearman's correlations (rho) are indicated. **(D)** Expression of the GSTP1 gene in various tumor tissues with paired normal tissues, shown in the GEP1A2 database. **(E)** Representative figures of tissue microarray staining for GSTP1 in normal ovarian tissue and OC tissues. **(F)** Western blot analysis of expression of GSTP1 in A2780 cells treated with different concentrations of rhCOLIII (0, 2, 4, and 8 mg/ml). **(G)** Western blot for validating the knockdown and overexpression of GSTP1 in A2780 cells. **(H)** Confocal microscopy and immunofluorescence assay showing intracellular site of GSTP1 and rhCOLIII. Biotin alone and unlabeled rhCOLIII were controls. Scale bar = 10 μm. **(I)** Transmission electron microscopy showing the subcellular structure of A2780 cells treated with rhCOLIII at different time points (0, 6, 12, and 24 h). Scale bar = 500 nm. Data are presented as mean ± SD of three independent experiments. The symbols *, **, and *** show $P < 0.05$, 0.01, and 0.001 versus the control group.

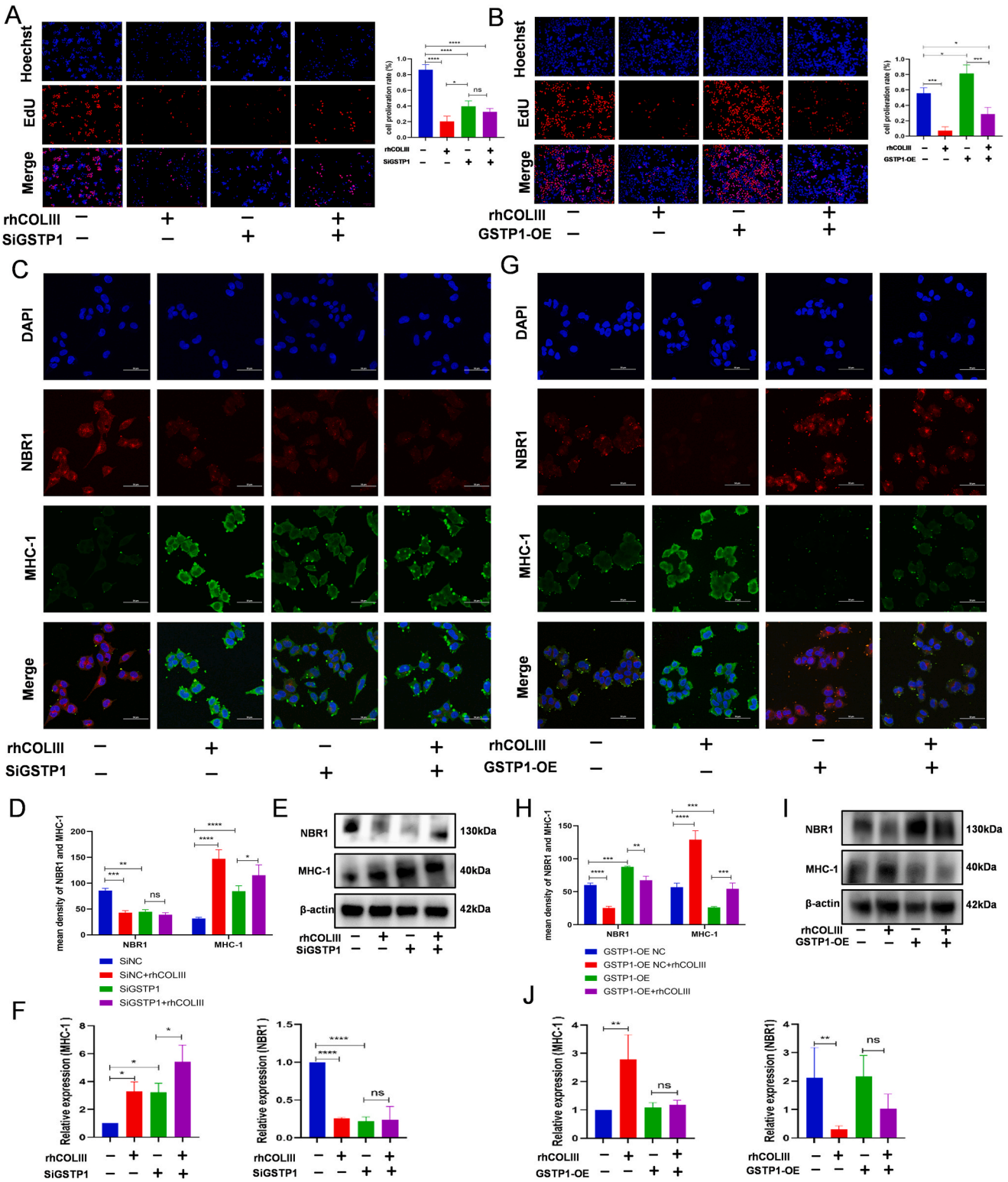

Fig. 5. rhCOLIII specifically inhibited autophagy and immune escape by regulating GSTP1 expression. **(A)** Proliferation ratio of A2780 cells was determined by EdU assay in the SiNC group, the rhCOLIII group, the GSTP1 KD group and the GSTP1 KD cells treated with rhCOLIII group. Scale bar = 100 μm. **(B)** Proliferation ratio of A2780 cells was determined by EdU assay in the GSTP1-OE NC group, the rhCOLIII group, the GSTP1 OE group and the GSTP1 OE cells treated with rhCOLIII group. Scale bar = 100 μm. **(C, D)** Representative images of immunofluorescence double staining of both NBR1 (red) and MHC-1 (green) in the SiNC group, the rhCOLIII group, the GSTP1 KD group and the GSTP1 KD cells treated with rhCOLIII group. Scale bar = 50 μm. **(E, F)** Western blot analysis of MHC-1 and NBR1 expression in the SiNC group, the rhCOLIII group, the GSTP1 KD group and the GSTP1 KD cells treated with rhCOLIII group. **(G, H)** Representative images of immunofluorescence double staining of both NBR1 (red) and MHC-1 (green) in the GSTP1-OE NC group, the rhCOLIII group, the GSTP1 OE group and the GSTP1 OE cells treated with rhCOLIII group. Scale bar = 50 μm. **(I, J)** Western blot analysis of MHC-1 and NBR1 expression in the GSTP1-OE NC group, the rhCOLIII group, the GSTP1 OE group and the GSTP1 OE cells treated with rhCOLIII group. (For interpretation of the references to colour in this figure legend, the reader is referred to the Web version of this article.)

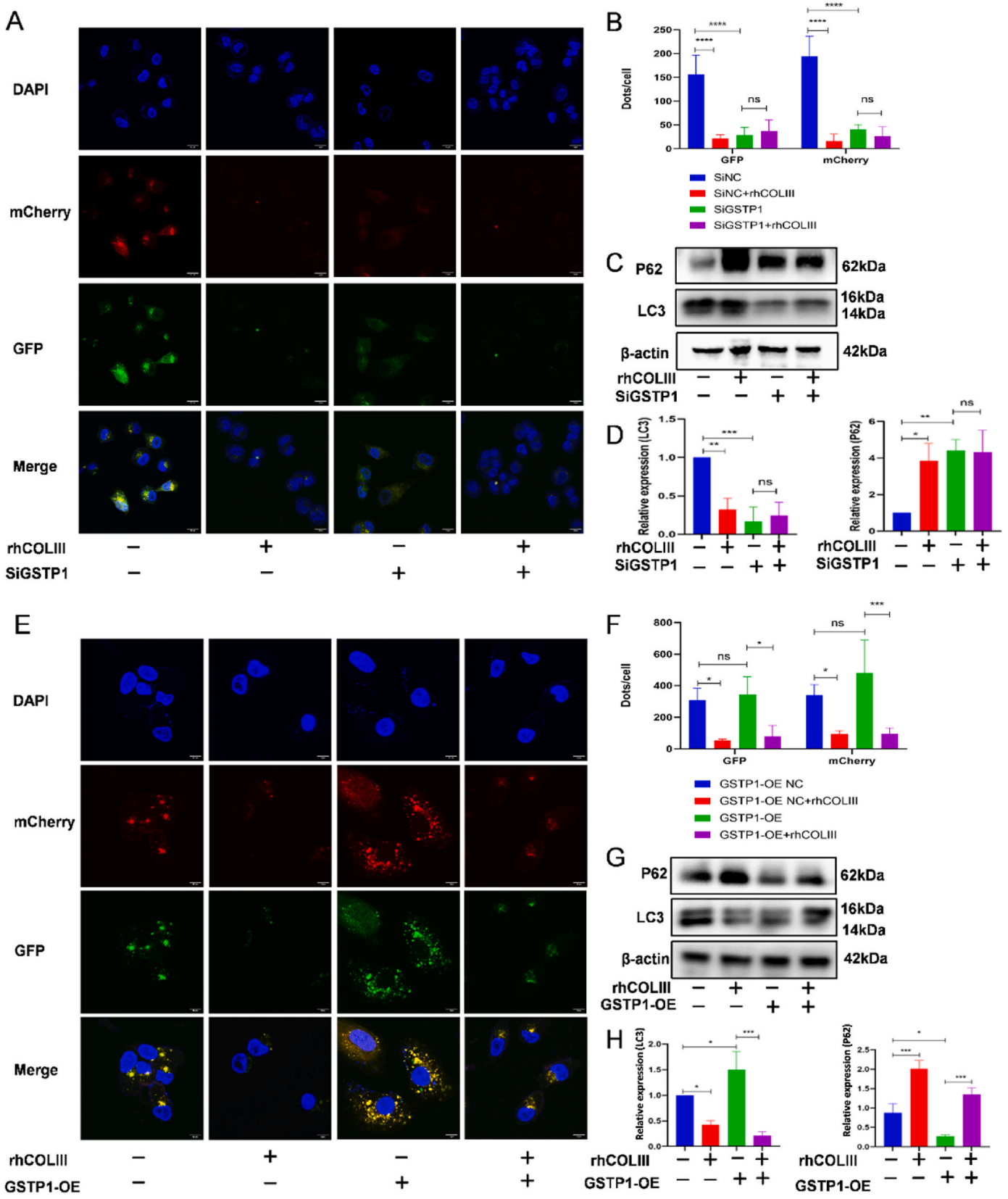

Fig. 6. rhCOLIII specifically inhibited autophagy and immune escape by regulating GSTP1 expression. **(A, B)** Autophagy flux, measured by confocal microscopy and quantification of intracellular LC3 dots in the SiNC group, the rhCOLIII group, the GSTP1 KD group and the GSTP1 KD cells treated with rhCOLIII group. Scale bar = 10 μm. **(C, D)** Western blot analysis of P62 and LC3 expression in the SiNC group, the rhCOLIII group, the GSTP1 KD group and the GSTP1 KD cells treated with rhCOLIII group. **(E, F)** Autophagy flux, measured by confocal microscopy and quantification of intracellular LC3 dots in the GSTP1-OE NC group, the rhCOLIII group, the GSTP1 OE group and the GSTP1 OE cells treated with rhCOLIII group. Scale bar = 10 μm. **(G, H)** Western blot analysis of P62 and LC3 expression in the GSTP1-OE NC group, the rhCOLIII group, the GSTP1 OE group and the GSTP1 OE cells treated with rhCOLIII group.

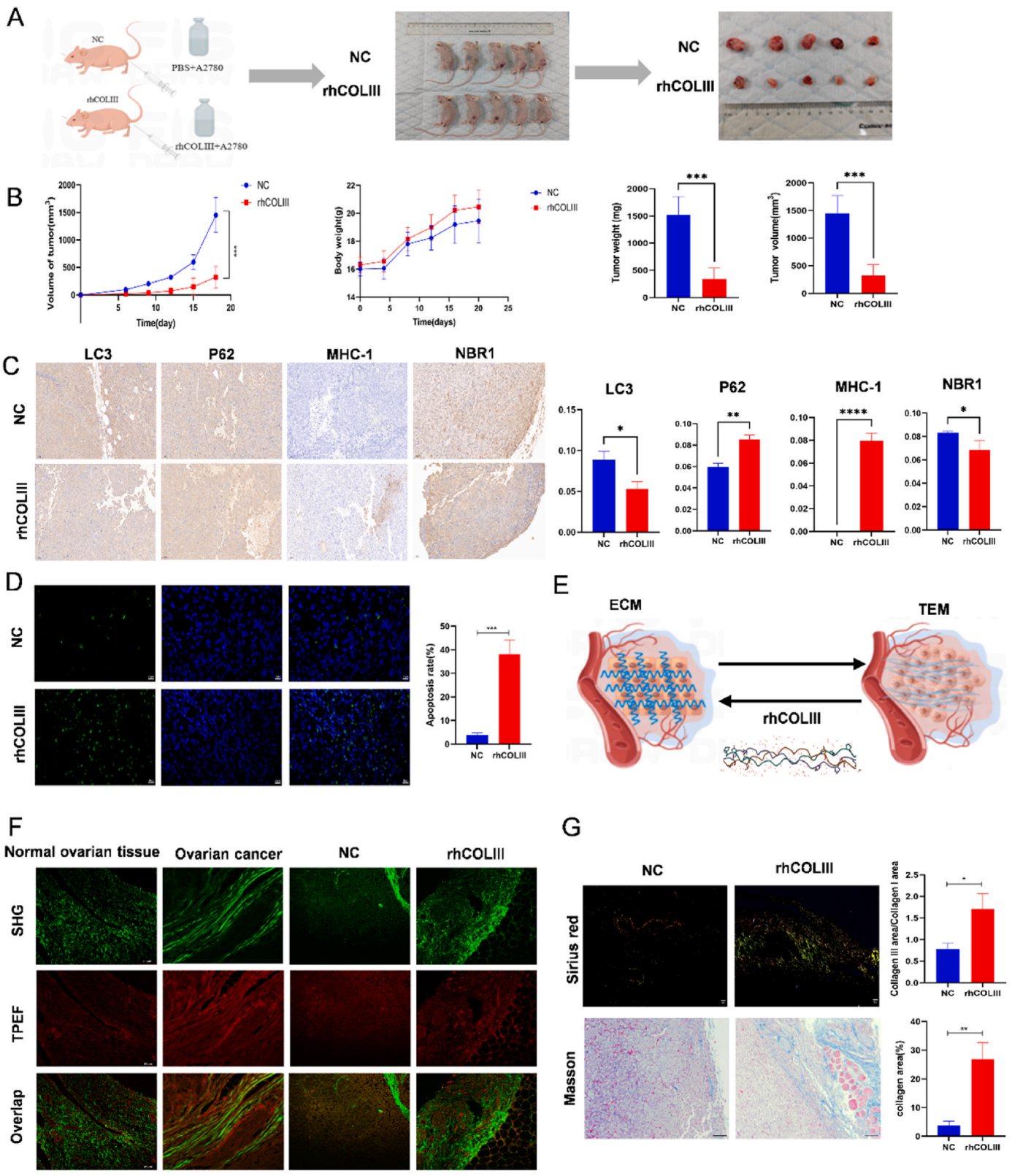

Fig. 7. rhCOLIII inhibited tumor growth, positively regulated immunity and remodeled extracellular matrix (ECM) *in vivo*. **(A, B)** Tumor volume was measured every three days and tumors were excised when the animals were sacrificed. Change in tumor over time in the two groups of nude mice. Quantification of tumor weight and volume in the control and rhCOLIII groups. **(C)** Immunohistochemical results of subcutaneous tumor tissue in nude mice, including P62, NBR1, LC3, MHC-1 expression. Scale bar = 50 μm. **(D)** TUNEL staining of subcutaneous tumor tissue in rhCOLIII treated mice and controls. Scale bar = 20 μm. **(E)** Schematic representation of normal ECM and TEM treated with rhCOLIII. **(F)** Representative SHG images from OC patients and patients with non-ovarian tumors, and SHG imaging in nude mouse model showing budding OC tissue in rhCOLIII treated and control groups. Scale bar = 80 μm. **(G)** Sirius red staining (Scale bar = 5 μm) and Masson trichrome staining (Scale bar = 50 μm) of subcutaneous tumor tissue. (For interpretation of the references to colour in this figure legend, the reader is referred to the Web version of this article.)

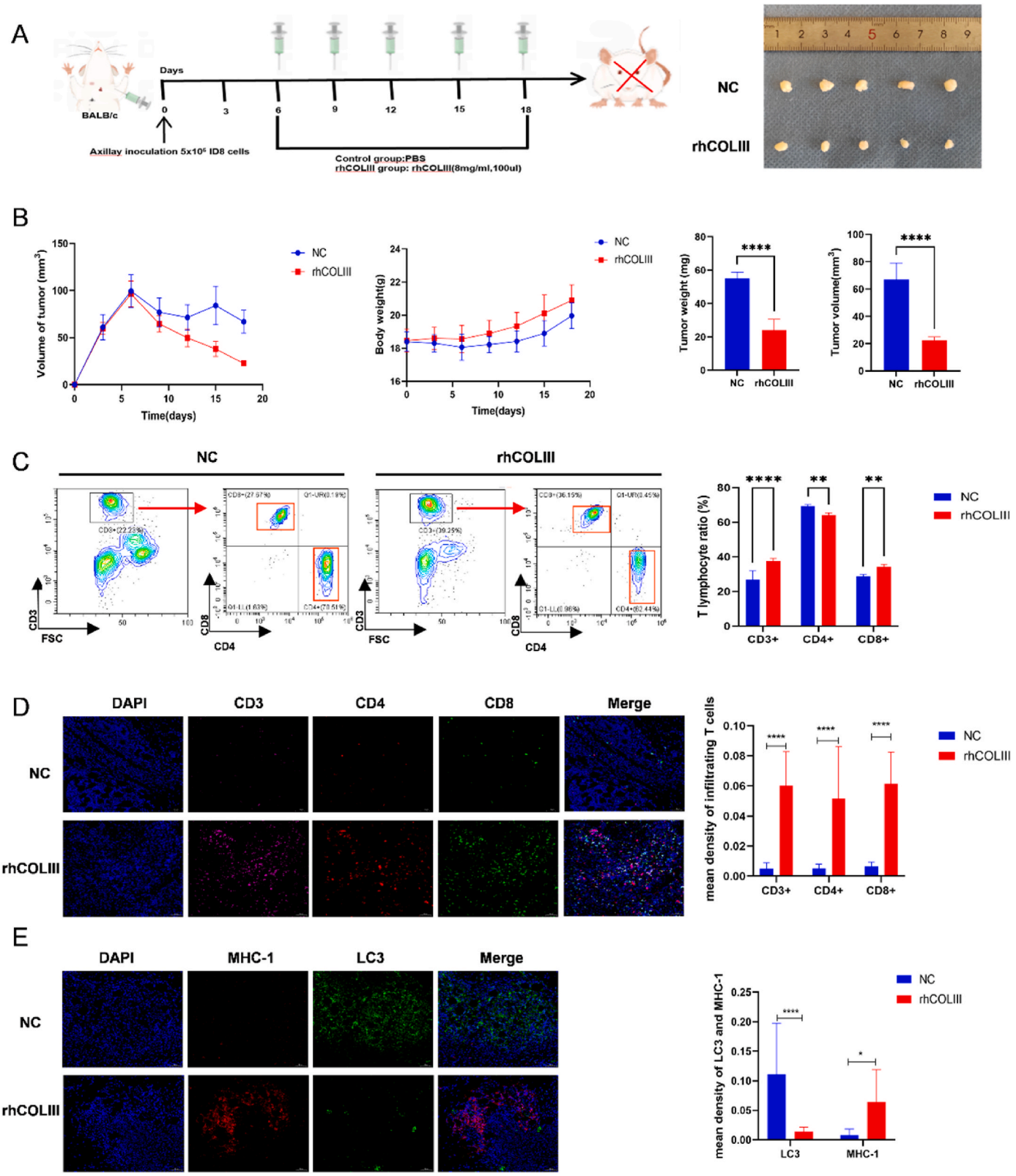

Fig. 8. rhCOLIII inhibited tumor growth, positively regulated immunity and remodeled extracellular matrix (ECM) *in vivo*. **(A, B)** BALB/C mice were inoculated with ID8 cells under their armpits, and after 5 days PBS (control) or rhCOLIII were administered at intervals of 3 days, change in mouse weight and axillary tumor volume is shown every three days. **(C)** Flow cytometry analysis of the proportion of $CD3^+$, $CD4^+$, $CD8^+$ T cells from the peripheral venous blood of BALB/C mice in the two groups. **(D)** Multiplex immunofluorescence staining of CD3, CD4, CD8 in mouse tumor tissue. Scale bar = 50 μm. **(E)** Immunofluorescence double staining of LC3 and MHC-1 in tumor tissue. Scale bar = 50 μm. Data are presented as mean ± SD of three independent experiments. The symbols * and ** show $P < 0.05$ and 0.01 versus the control group, respectively.

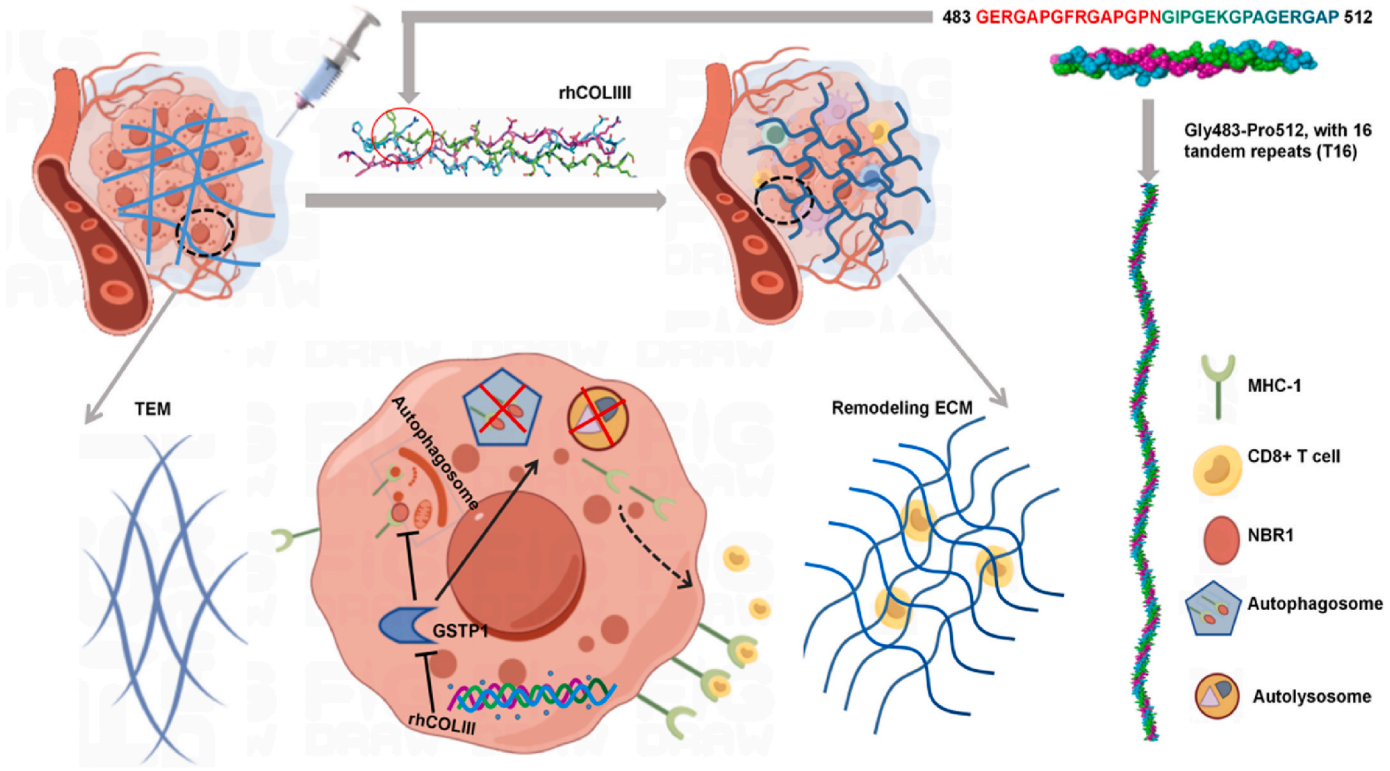

Fig. 9. Schematic illustration of rhCOLIII for autophagy inhibition and immune upregulation through GSTP1 in OC.

autophagy involvement, proteome and transcriptome combined analysis was performed showing that GSTP1 was significantly reduced. GSTP1, a phase II metabolic enzyme, plays a vital role in tumor cell signaling, metabolism, and drug resistance [34–36]. The TCGA database suggests that GSTP1 is associated with collagen formation and the autophagy pathway. Therefore, we speculate that rhCOLIII may inhibit the malignant behavior of OCCs mediated via GSTP1. Subsequetly, the gene GSTP1was overexpressed and knocked down in A2780 cells to conduct rescue experiments on proliferation, migration, invasion and autophagy. Taken together, these results demonstrated that rhCOLIII exerts anticancer effects and autophagy inhibition through down-regulation of GSTP1.

However, the specific mechanism of rhCOLIII in regulating GSTP1 expression is unclear. It is interesting that the immunofluorescence indicated that rhCOLIII was probably colocalized with GSTP1. Therefore, we hypothesize that there may be some relationship between rhCOLIII and GSTP1. Previous published studies established that GSTP1 belonged to a family of detoxification proteins referred to as glutathione *S*-transferases (GSTs) that catalyze the conjugation of GSH to electrophiles, and which was frequently overexpressed in tumors [37–39]. A recent study reported that the plant compound piperlongumine (PL) initiated the formation of a PL-GSH conjugate by occupying the hydrophobic region of the active site adjacent to GSH, the H-site. The PL-GSH conjugate inhibited GSTP1 and also cancer cell proliferation [40]. rhCOLIII may promote secretion of GSH, an antioxidant that reduces oxidative stress, which exerts cytoprotective effects by conjugation with GSTP1. Another possible explanation for reduction in GSTP1 is that rhCOLIII promotes of the formation of GSTP1 and GSH conjugates. Additionally, in order to provide further evidence of colocalization of rhCOLIII with GSTP1, we performed the protein–protein docking (ZDOCK) experiment. The ZDOCK Score of rhCOLIII and GSTP1 was −1052.26. Comprehensive analysis revealed that GSTP1 and rhCOLIII could form a stable protein docking model (Supplementary Table S4). However, further experiments are needed to establish this relationship between rhCOLIII and GSTP1.

The ECM is recognized as constantly dynamic responding to changes in the systemic environment. Collagen, is the main component of the ECM. Its morphology, structure, arrangement, and the fiber density affect the ECM and the progression of tumors [29,39,41,42]. Previous studies have reported that the collagen morphology of the ECM in malignancies including breast, pancreatic, and liver cancers is rigid and disorderly in arrangement [43]. Another study observed the change in collagen phenotype during immunotherapy in mouse melanoma models, with SHG imaging showing collagen reorganization toward a healthy phenotype, including wider and curlier collagen fibers, with modestly higher collagen density [44]. These findings are consistent with our results of SHG imaging showing more curved and neatly arranged collagen structure in normal human ovarian compared to OC tissue. In addition, our *in vivo* study also convincingly demonstrated that rhCOLIII remodeled the TME, with more curved and relatively neatly arranged collagen. We attribute this action to the special characteristics of rhCOLIII. The stable triple helix structure of collagen determines its wide application in the biomedical field [45]. Recombinant DNA engineering technology has developed and upgraded the functional sequences of recombinant collagen combined with human collagen to produce a new biomaterial, retaining the stable triple helix structure on self-assembly. This technology ensures product safety, improved hydrophilicity, cell adhesion and biocompatibility, and greatly reduced immunogenicity [46,47]. Therefore, we consider that rhCOLIII remodeled ECM by inducing healthier phenotype of collagen in the TEM.

The morphology, structure, arrangement, and density of collagen fibers were closely related to T cell localization, motility, and function [48,49]. Randomly aligned and highly curved collagen may lead to an ECM with a relaxed meshwork affecting ECM tension homeostasis, promoting optimal lymphocyte motility. In addition, rhCOLIII was shown to regulate immune function due to enhanced biological activity, structural stability and self-assembly in various cell types, including immune cells [15,28,50]. Our *in vitro and in vivo* experiments also demonstrated that rhCOLIII inhibited immune escape and increased T cell infiltration through autophagy regulation. GSTP1, a key regulatory

protein for the function of rhCOLIII, is also associated with immunity. A recent study showed that benzyl isothiocyanate (BITC) induced gene expression of a T-helper-2 cytokine through GSTP1 [51]. Another study suggested that the protective mechanism of lipopolysaccharide (LPS) on macrophages was associated with GSTPI stimulation during chemotherapy [52]. To explore the effect of GSTP1 on immunity, we employed profiles from the TGGA database and the Tumor Immune Estimation Resource (TIMER) to assess immune cell infiltration. Greater GSTP1 expression was associated with significantly decreased infiltration of T cells, macrophages, and other immune cells in OC samples. This suggests that lower GSTP1 expression is linked to higher immune cell infiltration, thereby decreasing immune escape.

Our study has some limitations. Firstly, the triple-helical structure rhCOLIII and human type III collagen amino acid sequence, may have potentially recognize collagen receptors, and the mechanisms of action still merit further study. Secondly, further verification is needed to determine whether rhCOLIII exerts immunomodulatory effects related to the triple helix structure or by affecting collagen immune receptors. Thirdly, specific labeling of rhCOLIII is needed to clarify its precise distribution in the ECM and its structural and functional relationship to immune cells. Finally, MHC molecules mainly comprise MHC I and MHC II, differentially expressed genes were identified before and after rhCOLIII treatment using transcriptome sequencing and found to be mainly associated with three MHC-1 related genes and one MHC-II related gene, but our study mainly focus on MHC-1 and not all were studied.

5. Conclusion

In conclusion, our study showed that rhCOLIII inhibited the proliferation, migration and invasion of OC by inhibition of autophagy. Combined proteome and transcriptome sequencing analysis, showed that rhCOLIII inhibited autophagy by regulating GSTP1. In addition, rhCOLIII increased the expression of MHC-1 to overcome immune escape *in vitro* and induced protective anti-tumor immunity *in vivo*. Our findings suggest that rhCOLIII may be a very promising therapeutic approach to OC.

Funding

This study was funded by Taiyuan's "Open bidding for selecting the best candidates" Program (2024TYJB0149) and sponsored by Natural Science Foundation of Chongqing, China (CSTB2022NSCQ-MSX0087).

Ethics approval and consent to participate

All animal experiments were approved by the Institutional Animal Care and Use Committee of Chongqing Medical University. (Permit Number: IACUC-CQMU-2023-0308).

Consent for publication

Not applicable.

CRediT authorship contribution statement

Hui Zeng: Writing – original draft, Software, Methodology, Investigation, Formal analysis, Conceptualization. **Hu Li:** Writing – review & editing, Methodology, Data curation. **Li Wang:** Writing – review & editing, Methodology. **Shuang You:** Supervision, Project administration, Investigation, Conceptualization. **Shuaibin Liu:** Project administration, Investigation. **Xiaojing Dong:** Visualization, Software, Methodology, Data curation. **Fan He:** Visualization, Investigation, Formal analysis. **Jingcong Dai:** Visualization, Software, Methodology, Data curation. **Quan Wei:** Software, Formal analysis, Conceptualization. **Zhiyong Dong:** Software, Formal analysis, Data curation. **Yanli Zhang:** Resources, Project administration. **Jingbo Yang:** Visualization, Software, Resources. **Xia Yang:** Resources, Conceptualization. **Jian Wang:** Visualization, Investigation. **Lina Hu:** Supervision, Project administration, Data curation.

Declaration of competing interest

The authors declare that they have no known competing financial interests or personal relationships that could have appeared to influence the work reported in this paper.

Data availability

Data will be made available on request.

Acknowledgments

This work was supported by the Scientific and Technological Research Program of the Chongqing Municipal Education Commission (Grant No. KJCXZD2020017). We sincerely thank Shanxi Jinbo Bio-Pharmaceutical CO., Ltd. for their help in providing rhCOLIII and the Imaging Core Facility, Technology Center for Protein Science, Tsinghua University for their help in SHG imaging. In addition, we would like to express gratitude to EditSprings (https://www.editsprings.cn) for the expert linguistic services provided.

Abbreviations

OC	Ovarian cancer
rhCOLIII	recombinant humanized type III collagen
GSTP1	Glutathione S-transferase P1
TME	Tumor microenvironment
MHC-I	Histocompatibility complex class I
SHG	Second generation harmonic
NBR1	Neighbor of BRCA1 gene 1
siRNA	Small interfering RNA
LCM-MS	Liquid chromatography-tandem mass spectrometry
SEM	Scanning electron microscopy

Appendix A. Supplementary data

Supplementary data to this article can be found online at https://doi.org/10.1016/j.mtbio.2024.101220.

References

[1] X. Huang, X.Y. Li, W.L. Shan, Y. Chen, Q. Zhu, B.R. Xia, Targeted therapy and immunotherapy: diamonds in the rough in the treatment of epithelial ovarian cancer, Front. Pharmacol. 14 (2023 Mar 24) 1131342.
[2] Lheureux S, Gourley C, Vergote I, Oza AM. Epithelial ovarian cancer. Lancet. 2019 Mar 23;393(10177):1240-1253.
[3] D.G. Leach, S. Young, J.D. Hartgerink, Advances in immunotherapy delivery from implantable and injectable biomaterials, Acta Biomater. 88 (2019 Apr 1) 15–31.
[4] Y. Chao, C. Liang, H. Tao, Y. Du, D. Wu, Z. Dong, Q. Jin, G. Chen, J. Xu, Z. Xiao, Q. Chen, C. Wang, J. Chen, Z. Liu, Localized cocktail chemoimmunotherapy after in situ gelation to trigger robust systemic antitumor immune responses, Sci. Adv. 6 (10) (2020 Mar 4) eaaz4204.
[5] A.M. Diez-Pascual, A. Rahdar, Functional nanomaterials in biomedicine: current uses and potential applications, ChemMedChem 17 (16) (2022 Aug 17) e202200142.
[6] E. Pérez-Herrero, O.L. Lanier, N. Krishnan, A. D'Andrea, N.A. Peppas, Drug delivery methods for cancer immunotherapy, Drug Deliv Transl Res 14 (1) (2024 Jan) 30–61.
[7] M. Fang, J. Yuan, C. Peng, et al., Collagen as a double-edged sword in tumor progression, Tumor Biol. 35 (2014) 2871–2882.
[8] S. Xu, H. Xu, W. Wang, et al., The role of collagen in cancer: from bench to bedside, J. Transl. Med. 17 (2019) 1–22.
[9] J.S. Di Martino, A.R. Nobre, C. Mondal, I. Taha, E.F. Farias, E.J. Fertig, A. Naba, J. A. Aguirre-Ghiso, J.J. Bravo-Cordero, A tumor-derived type III collagen-rich ECM niche regulates tumor cell dormancy, Nat. Can. (Ott.) 3 (1) (2022 Jan) 90–107.
[10] E.I. Harper, T.S. Hilliard, E.F. Sheedy, P. Carey, P. Wilkinson, M.D. Siroky, J. Yang, E. Agadi, A.K. Leonard, E. Low, Y. Liu, A. Biragyn, C.M. Annunziata, M.S. Stack,

Another wrinkle with age: aged collagen and intra-peritoneal metastasis of ovarian cancer, Aging Cancer 3 (2) (2022 Jun) 116–129.
[11] S. Chattopadhyay, R.T. Raines, Review collagen-based biomaterials for wound healing, Biopolymers 101 (8) (2014 Aug) 821–833.
[12] A. Rahman, T.H. Silva, Collagens from marine organisms towards biomedical applications, Mar. Drugs 20 (2022) 170.
[13] Y. Xu, M. Kirchner, Collagen mimetic peptides, Bioengineering (Basel) 8 (1) (2021 Jan 5) 5.
[14] C. Hua, Y. Zhu, W. Xu, S. Ye, R. Zhang, L. Lu, S. Jiang, Characterization by high-resolution crystal structure analysis of a triple-helix region of human collagen type III with potent cell adhesion activity, Biochem. Biophys. Res. Commun. 508 (4) (2019 Jan 22) 1018–1023.
[15] S. You, Y. Zhu, H. Li, F. He, S. Liu, X. Yang, L. Wang, H. Zeng, J. Dai, L. Hu, Recombinant humanized collagen remodels endometrial immune microenvironment of chronic endometritis through macrophage immunomodulation, Regen Biomater 10 (2023) rbad033. Apr3.
[16] S. You, S. Liu, X. Dong, H. Li, Y. Zhu, L. Hu, Intravaginal administration of human type III collagen-derived biomaterial with high cell-adhesion activity to treat vaginal atrophy in rats, ACS Biomater. Sci. Eng. 6 (2020) 1977–1988.
[17] H. Li, S. You, X. Yang, et al., Injectable recombinant human collagen-derived material with high cell adhesion activity limits adverse remodeling and improves pelvic floor function in pelvic floor dysfunction rats, Biomater. Adv. 134 (2022) 112715.
[18] X. Liu, H. Li, T. Wang, T. Yang, X. Yang, K. Guo, L. Hu, J. Ming, Recombinant humanized collagen type III with high antitumor activity inhibits breast cancer cells autophagy, proliferation, and migration through DDR1, Int. J. Biol. Macromol. 243 (2023 Jul 15) 125130.
[19] X. Zhang, M. Zhang, H. Cui, T. Zhang, L. Wu, C. Xu, C. Yin, J. Gao, Autophagy-modulating biomembrane nanostructures: a robust anticancer weapon by modulating the inner and outer cancer environment, J. Contr. Release 366 (2024 Feb) 85–103.
[20] K. Yamamoto, A. Venida, J. Yano, et al., Autophagy promotes immune evasion of pancreatic cancer by degrading MHC-I, Nature 581 (7806) (2020 May) 100–105.
[21] Mechanisms of transcoelomic metastasis in ovarian cancer, D.S. Tan, R. Agarwal, S. B. Kaye, Lancet Oncol. 7 (2006) 925–934.
[22] Ovarian cancer spheroids use myosin-generated force to clear the mesothelium, M. P. Iwanicki, R.A. Davidowitz, M.R. Ng, et al., Cancer Discov. 1 (2011) 144–157.
[23] C. Ricciardelli, R.J. Rodgers, Extracellular matrix of ovarian tumors, Semin. Reprod. Med. 24 (4) (2006 Sep) 270–282.
[24] R. Borst, L. Meyaard, M.I. Pascoal Ramos, Understanding the matrix: collagen modifications in tumors and their implications for immunotherapy, J. Transl. Med. 22 (1) (2024 Apr 24) 382.
[25] D.E. Desa, R.L. Strawderman, W. Wu, et al., Intratumoral heterogeneity of second-harmonic generation scattering from tumor collagen and its effects on metastatic risk prediction, BMC Cancer 20 (1) (2020 Dec 10) 1217.
[26] M. Fang, J. Yuan, C. Peng, et al., Collagen as a double-edged sword in tumor progression, Tumor Biol. 35 (2014) 2871–2882.
[27] S. Xu, H. Xu, W. Wang, et al., The role of collagen in cancer: from bench to bedside, J. Transl. Med. 17 (2019) 1–22.
[28] A. Gertych, A.E. Walts, K. Cheng, et al., Dynamic changes in ECM in primary, metastatic, and recurrent ovarian cancers, Cells 11 (23) (2022) 3769. Nov 25.
[29] A. Mancini, M.T. Gentile, F. Pentimalli, S. Cortellino, M. Grieco, A. Giordano, Multiple aspects of matrix stiffness in cancer progression, Front. Oncol. 14 (2024 Jul 2) 1406644.
[30] B.K. Brisson, E.A. Mauldin, W. Lei, et al., Type III collagen directs stromal organization and limits metastasis in a murine model of breast cancer, Am. J. Pathol. 185 (5) (2015 May) 1471–1486.
[31] S. Kauppila, M.K. Bode, F. Stenbäck, et al., Cross-linked telopeptides of type I and III collagens in malignant ovarian tumours in vivo, Br. J. Cancer 81 (4) (1999 Oct) 654–661.
[32] C. Hua, Y. Zhu, W. Xu, et al., Characterization by high-resolution crystal structure analysis of a triple-helix region of human collagen type III with potent cell adhesion activity, Biochem. Biophys. Res. Commun. 508 (4) (2019 Jan 22) 1018–1023.
[33] J. Wang, H. Qiu, Y. Xu, et al., The biological effect of recombinant humanized collagen on damaged skin induced by UV-photoaging: an in vivo study, Bioact. Mater. 11 (2021 Oct 22) 154–165.
[34] X. Dong, Y. Yang, Y. Zhou, X. Bi, N. Zhao, Z. Zhang, L. Li, Q. Hang, R. Zhang, D. Chen, P. Cao, Z. Yin, L. Luo, Glutathione S-transferases P1 protects breast cancer cell from adriamycin-induced cell death through promoting autophagy, Cell Death Differ. 26 (10) (2019 Oct) 2086–2099.
[35] B. Mannervik, V.M. Castro, U.H. Danielson, M.K. Tahir, J. Hansson, U. Ringborg, Expression of class Pi glutathione transferase in human malignant melanoma cells, Carcinogenesis 8 (1987) 1929–1932.
[36] B. Cheng, Y. Wang, A.A. Ayanlaja, et al., Glutathione S-transferases S1, Z1 and A1 serve as prognostic factors in glioblastoma and promote drug resistance through antioxidant pathways, Cells 11 (20) (2022 Oct 14) 3232.
[37] J.D. Hayes, D.J. Pulford, The glutathione S-transferase supergene family: regulation of GST and the contribution of the isoenzymes to cancer chemoprotection and drug resistance, Crit. Rev. Biochem. Mol. Biol. 30 (1995) 445–600.
[38] G. Guerrero-Barberà, N. Burday, M. Costell, Shaping oncogenic microenvironments: contribution of fibronectin, Front. Cell Dev. Biol. 12 (2024 Apr 10) 1363004.
[39] P.G. Board, M. Coggan, G. Chelvanayagam, et al., Identification, characterization, and crystal structure of the Omega class glutathione transferases, J. Biol. Chem. 275 (32) (2000 Aug 11) 24798–24806.
[40] W. Harshbarger, S. Gondi, S.B. Ficarro, et al., Structural and biochemical analyses reveal the mechanism of glutathione S-transferase pi 1 inhibition by the anti-cancer compound piperlongumine, J. Biol. Chem. 292 (1) (2017 Jan 6) 112–120.
[41] Y. Liu, K.W. Eliceiri, Quantifying fibrillar collagen organization with curvelet transform-based tools, J. Vis. Exp. (165) (2020 Nov 11).
[42] W. Xie, X. Wei, H. Kang, et al., Static and dynamic: evolving biomaterial mechanical properties to control cellular mechanotransduction, Adv. Sci. 10 (9) (2023 Mar) e2204594.
[43] J. Prakash, Y. Shaked, The interplay between extracellular matrix remodeling and cancer therapeutics, Cancer Discov. 14 (8) (2024 Aug 2) 1375–1388.
[44] A.R. Heaton, N.J. Burkard, P.M. Sondel, M.C. Skala, Quantifying in vivo collagen reorganization during immunotherapy in murine melanoma with second harmonic generation imaging, Biophotonics Discov 1 (1) (2024 May) 015004.
[45] B. An, Y. Wang, Y. Huang, X. Wang, Y. Liu, D. Xun, G.M. Church, Z. Dai, X. Yi, T. C. Tang, C. Zhong, Engineered living materials for sustainability, Chem. Rev. 123 (5) (2023 Mar 8) 2349–2419.
[46] J. Sun, J. Su, C. Ma, R. Göstl, A. Herrmann, K. Liu, H. Zhang, Fabrication and mechanical properties of engineered protein-based adhesives and fibers, Adv. Mater. 32 (6) (2020 Feb) e1906360.
[47] A.M. Diez-Pascual, A. Rahdar, Functional nanomaterials in biomedicine: current uses and potential applications, ChemMedChem 17 (16) (2022 Aug 17) e202200142.
[48] C. Zeltz, M. Kusche-Gullberg, R. Heljasvaara, D. Gullberg, Novel roles for cooperating collagen receptor families in fibrotic niches, Curr. Opin. Cell Biol. 85 (2023 Dec) 102273.
[49] X. Chen, Q. Wu, Z. Gong, et al., A natural plant ingredient, menthone, regulates T cell subtypes and lowers pro-inflammatory cytokines of rheumatoid arthritis, J. Nat. Prod. 85 (4) (2022 Apr 22) 1109–1117.
[50] D.G. Leach, S. Young, J.D. Hartgerink, Advances in immunotherapy delivery from implantable and injectable biomaterials, Acta Biomater. 88 (2019 Apr 1) 15–31.
[51] Y. Tang, S. Naito, N. Abe-Kanoh, S. Ogawa, S. Yamaguchi, B. Zhu, Y. Murata, Y. Nakamura, Benzyl isothiocyanate attenuates the hydrogen peroxide-induced interleukin-13 expression through glutathione S-transferase P induction in T lymphocytic leukemia cells, J. Biochem. Mol. Toxicol. 32 (6) (2018 Jun) e22054.
[52] S. Song, X. Zhang, L. Cui, Y. Wang, X. Tian, K. Wang, K. Ji, Mechanisms of lipopolysaccharide protection in tumor drug-induced macrophage damage, Int. J. Biol. Macromol. 266 (Pt 2) (2024 May) 131006.